TOPICAL REVIEW

Directed self-assembly of block copolymers for use in bit patterned media fabrication

Rhys Alun Griffiths[1,2]**, Aled Williams**[2]**, Chloe Oakland**[2]**, Jonathan Roberts**[2]**, Aravind Vijayaraghavan**[1] **and Thomas Thomson**[1]

[1] School of Computer Science, The University of Manchester, Manchester, M13 9PL, UK
[2] Northwest Nanoscience Doctoral Training Centre (NOWNano DTC), The University of Manchester, Manchester, M13 9PL, UK

E-mail: rhys.griffiths-2@postgrad.manchester.ac.uk

Abstract

Reduction of the bit size in conventional magnetic recording media is becoming increasingly difficult due to the superparamagnetic limit. Bit patterned media (BPM) has been proposed as a replacement technology as it will enable hard disk areal densities to increase past $1\,\mathrm{Tb\,in^{-2}}$. Block copolymer directed self-assembly (BCP DSA) is the leading candidate for forming BPM due to its ability to create uniform patterns over macroscopic areas. Here we review the latest research into two different BCP DSA techniques: graphoepitaxy and chemoepitaxy (or chemical prepatterning). In addition to assessing their potential for forming high density bit patterns, we also review current approaches using these techniques for forming servo patterns, which are required for hard disk drive (HDD) operation. Finally, we review the current state of UV nanoimprint lithography, which is the favoured technique for enabling mass production of BPM HDDs.

(Some figures may appear in colour only in the online journal)

1. Introduction

Magnetic data storage can trace its origins back to the invention of the magnetic wire recorder in 1898 by Valdemar Poulsen [1]. These early devices relied on analogue recording to create the time varying signal necessary to reproduce sound waves. The advent of the digital electronic computer created a need for digital recording. The key concept of digital magnetic data storage is the ability of a small region of material to be in one of two well defined magnetic states. This corresponds to a binary digit. These well defined states occur naturally in magnetic materials with uniaxial anisotropy, and their magnetization can be flipped by the application of a magnetic field. IBM used this idea in 1956 to create the first hard disk drive (HDD), with a bit areal density of $2\,\mathrm{kB\,in^{-2}}$ [2]. Since then, bit areal densities have increased exponentially, reaching $635\,\mathrm{Gb\,in^{-2}}$ in 2010 [3]—a 317.5 million fold increase in the space of 54 years.

In a modern HDD, the material in which the magnetic data are stored is rotated beneath a recording head which is moved by an actuator across the medium, allowing the head to read or write data across concentric circular tracks. The magnetic data storage media consists of a highly optimized nano-granular magnetic thin film, which is sputter coated onto both sides of the disk substrate [4]. The film stack typically includes soft underlayers ($\sim 30\,\mathrm{nm}$), various seed layers ($\sim 40\,\mathrm{nm}$), a
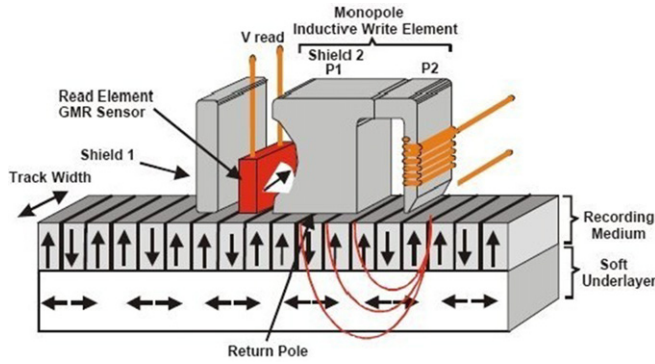
Figure 1. Schematic diagram of a head flying over a perpendicularly magnetized recording medium. Each up or down arrow in the recording medium represents a bit. Used with permission from HGST.

magnetic data storage film ($\sim$12–15 nm), and a thin protective carbon overcoat ($\sim$3 nm) [5]. A thin layer of lubricant ($\sim$1 nm) is applied to the surface.

The current technology used in HDDs is perpendicular recording [6], shown schematically in figure 1. Each up or down arrow represents a bit, and consists of fewer than one hundred nanoscale ($\sim$8 nm diameter) grains. The film is deposited so that there is only weak exchange coupling between grains, in order to achieve narrow bit boundaries [7]. Each grain has a perpendicular easy axis, meaning that the field from the write-head can set the magnetization of the grains in each bit to point 'up' or 'down' relative to the plane of the disk. Data are read back by moving the read-head along the track and detecting the magnetic flux that collectively emanates from the grains that comprise each bit.

Increases in storage density are achieved by reducing the area taken up by each bit. One method is to reduce the number of grains that are contained in an individual bit. However, future reduction is limited due to the requirement that the recording system has an adequate signal-to-noise ratio (SNR), which is proportional to the number of magnetic grains per bit [8]. A second method is to reduce the grain size. Historically, this has been the key driver of areal density growth, although recently this trend has faltered as it has become increasingly difficult to produce grains smaller than 8–9 nm with narrow size distributions and narrow distributions of magnetic properties.

The energy barrier that separates a grain's two stable magnetization states is approximately equal to $K_u V$, where K_u is the magnetic anisotropy of the material, and V is the grain volume. Therefore as the grain volume is reduced, the energy barrier becomes lower. When the size of the barrier becomes comparable to the thermal energy, $k_B T$, thermal fluctuations can spontaneously flip the magnetization of the grain. For a HDD to retain information for 10 years, a widely used metric is that $K_u V / k_B T > 60$ is required [9]. Therefore this physical limit, termed the superparamagnetic limit, sets a boundary on further decreases in grain size. Further decreases in V would be possible if the value of K_u was increased by using a recording material with higher anisotropy. However, that leads to the problem of writability, as there is a limit to the write field that can be produced based on the available write-head
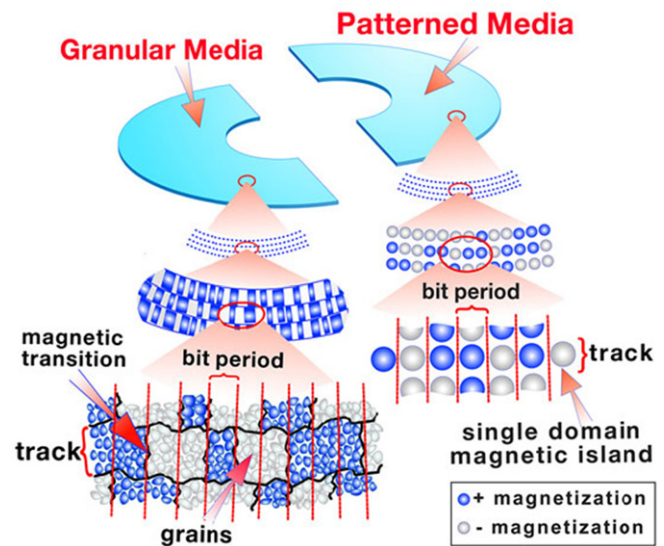

Figure 2. A schematic of how bits are stored in conventional granular media and BPM. Used with permission from HGST.

materials [7]. These three conflicting requirements between SNR, thermal stability, and writability, popularly termed the magnetic recording trilemma [10], are hindering further areal density growth. The highest storage density that can be achieved with perpendicular media is predicted to be 1 Tb in^{-2}, after which further areal density increases will require a new storage technology.

There are two main approaches to enable growth beyond 1 Tb in^{-2}. The first, termed heat assisted magnetic recording (HAMR) [11], is focused on increasing the value of K_u. To enable the write-head field to switch the magnetization, the coercivity can be reduced immediately prior to writing by heating the bit with, for example, a laser. The introduction of HAMR whilst still using conventional granular media has been predicted to raise the storage density limit to between 3 and 5 Tb in^{-2} [12]. However, in practice this is proving very difficult to achieve, in part due to the difficulties of continuing to scale the grain size in conventional granular media, and despite a significant research and development effort, reliable demonstrations have yet to reach 1 Tb in^{-2}.

The second approach, termed bit patterned media (BPM), offers a true alternative. Here thermal stability is obtained by increasing the value of V, and this is explored in the next section.

2. Bit patterned media

The concept of BPM is to pattern a magnetic film into individual islands, where each magnetic island stores one bit. Figure 2 shows a schematic of the difference between bits stored in conventional granular media and BPM. As the bit boundaries are defined physically by the boundary of each island, the original film can be deposited so that there is strong exchange coupling between the individual grains within an island. This coupling results in V being the volume of the island instead of the volume of an individual grain [13], allowing the size of a bit to be decreased, whilst

still maintaining thermal stability and producing an adequate SNR. If introduced using conventional write-head technology, BPM is estimated to enable areal densities up to $5\,\text{Tb}\,\text{in}^{-2}$ before writability becomes an issue [14]. For a combined HAMR-BPM system, estimates of the maximum possible areal density range from $20\,\text{Tb}\,\text{in}^{-2}$ [15] to $100\,\text{Tb}\,\text{in}^{-2}$ [16] using FePtX media, and up to $300\,\text{Tb}\,\text{in}^{-2}$ in an idealized case using SmCo media [17]. However mass producing arrays of nano-sized magnetic islands is not an easy task, and the requirements placed on their properties are stringent.

The topographical requirements are that the placement and size of each bit must be precise. Accurate placement is required to achieve write synchronization between the read/write-head and the underlying bits. Bit size must not be so great that adjacent bits touch and magnetically couple, and not so small that the bit becomes superparamagnetic [18]. Both the bit placement distribution and size distribution must be no greater than 5% (1σ) [19, 20].

The magnetic requirements are that the switching field of each bit (the field that must be applied to flip the magnetization) must fall within a narrow range. A wide switching field distribution (SFD) would mean that the write field could not flip the magnetization of high anisotropy bits. This could be overcome by using a higher write field, but this is limited by the field that write-heads can practically produce, and also by the requirement that the write field is not so strong as to accidentally overwrite an adjacent bit, which could have a lower switching field.

The primary contributor to SFD broadening is an intrinsic variation of anisotropy in the thin film from which the bits are fashioned [21, 22]. However variations in island shape, size, and edge defects will also cause SFD broadening. Therefore realization of a narrow SFD will require optimization of the film deposition, patterning and etching processes. One additional factor that contributes to SFD broadening is dipolar interactions from adjacent bits. This can be reduced by decreasing the magnetic moments of the bits, although a certain magnetic moment is required for the read-head to be able to detect them [23].

The focus of this review is to examine the progress towards achieving mass production of BPM platters that meet the bit placement and size distribution requirements. However the tuning of the magnetic film properties in order to reduce the SFD of the bits is also a significant challenge that must be overcome.

2.1. Top down assembly

The technique most commonly used to produce nanoscale patterns over a large area is lithography. Various forms of lithography exist and can be used to fabricate the structures needed for BPM. Examples of these are photolithography, interference lithography (IL), and electron beam lithography. In these methods, a resist is exposed to a particular type of radiation, creating a pattern which can then be transferred to a magnetic film. For $1\,\text{Tb}\,\text{in}^{-2}$ BPM, dots would need to be patterned with a period (dot centre–dot centre distance) of $\sim$25 nm, and a dot diameter of 12.5 nm for 50% linear filling

factor, or 15–18.75 nm for more commonly seen 60–75% linear filling factors.

Photolithography is the primary lithography technique used by the semiconductor industry. UV light is shone through an optical mask to transfer the pattern onto an underlying resist. It cannot produce features smaller than the diffraction limit, determined by the numerical aperture of the optics and the wavelength of light being used. However its resolution can be enhanced by using immersion lithography, where the gap between the final lens and wafer surface is filled by a liquid medium with a refractive index greater than 1, and also by using multiple patterning techniques. The current industry standard wavelength of 193 nm has achieved feature sizes of 19 nm [24]. Feature sizes required by patterned media could potentially be produced using extreme ultraviolet (EUV) lithography with 13.5 nm wavelength, which is likely to be the next technology used by the semiconductor industry [25]. However the required island size is more than 2× smaller than what the semiconductor industry is targeting for the rest of this decade, and the large volume required (roughly 1 billion disks per year) compared with the much smaller total number of wafers produced by the semiconductor industry means this would likely be a very expensive option for patterned media [26].

An alternative solution could be to use IL, where a pattern of fringes is produced using two interfering optical beams [5]. The advantage of this technique is that periodic patterns can be produced over large areas without needing a corresponding optical mask. Solak and Ekinci [27] have demonstrated a $1\,\text{Tb}\,\text{in}^{-2}$ hole-array pattern in calixarene resist, as can be seen in figure 3(*a*). They believe that an ultimate density of $13\,\text{Tb}\,\text{in}^{-2}$ could be achieved if resists of required resolution were developed. However, their technique, termed EUV-IL [28], also requires wavelengths smaller than those that can be produced with commercially available sources. For their work they used a synchrotron source, which would be unfeasible for mass production although could conceivably offer a route to the fabrication of master templates. Additionally, rotating disk storage requires arrays with circular symmetry which adds complication in generating the interference pattern. However, EUV-IL has demonstrated concentric circular light patterns through the interference of two spherical beams (where the spherical beams are created using Fresnel zone plates) [29], which could be used as a first step in creating BPM with circular symmetry.

The most established tool that has demonstrated consistent resolution below 25 nm is electron beam lithography (EBL) [4]. This writes a pattern into a resist with a directed beam of electrons [31]. This can typically pattern dots as small as 8 nm diameter, and has demonstrated a resolution of 2 nm under specialized conditions [32]. An array of $1.1\,\text{Tb}\,\text{in}^{-2}$ dots patterned into resist using EBL can be seen in figure 3(*b*).

The period of the bits created using this technique is limited by the proximity effect, which causes adjacent features to overlap due to the scattering of the electrons within the resist [33] and backscattering of electrons from the substrate. The accuracy of the patterns is determined by the stability of the instrument, both in terms of the mechanical stages
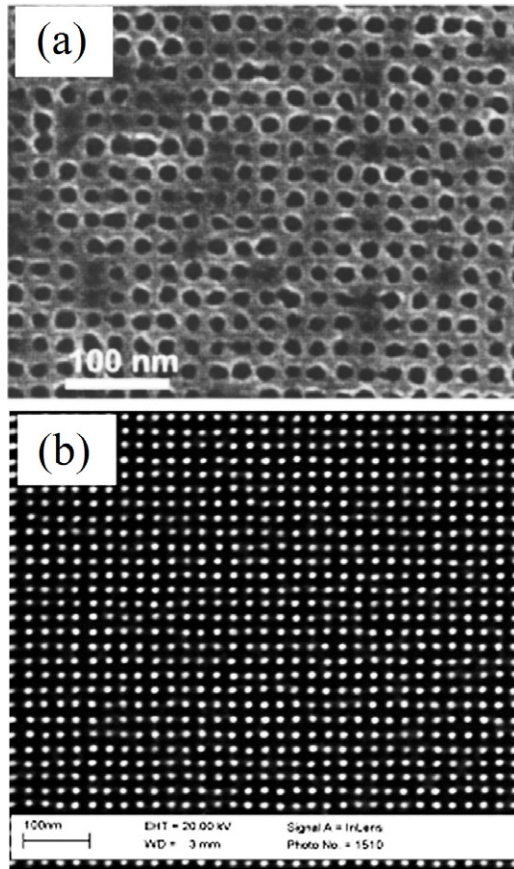
Figure 3. (*a*) SEM image of a square hole-array pattern with 25 nm period formed in calixarene resist using EUV-IL [27]. (*b*) SEM image of 30 nm thick HSQ resist patterned with pitch of 24 nm (~1.1 Tb in^{-2}) using EBL [30]. Figures reprinted with permission. Copyright 2007, American Vacuum Society.

Figure 4. Illustration of the UV nanoimprint process. (*a*) Resist is deposited onto a substrate, and a UV-transparent template is positioned above. (*b*) The template is pressed into the resist and UV light is shone through the template to cure the resist. (*c*) The template is released leaving the cured resist with the imprinted features.

(e.g. temperature stability of the cleanroom) and the electron deflection mechanism. Also EBL is a slow, serial technique, and clearly cannot meet the requirement of up to 1000 double-sided disks per hour [34]. However, if a master template could be fabricated using EBL, it could then be replicated many times using nanoimprint lithography (NIL) [35], a 1× replication technique where a master template is stamped into a resist. This dual EBL-NIL approach is the current focus of industry efforts to enable mass production of BPM HDDs. NIL is introduced below before section 9 provides an in-depth survey of current capabilities.

2.1.1. Nanoimprint lithography. NIL is a 1× lithography where a template is pressed into a material in order to form a pattern. Several nanoimprinting processes have been reported in the literature, including thermal imprint lithography [35] and ultraviolet (UV) cure imprint lithography [36]. A comprehensive review was given by Schift [37]. UV cure NIL is presently the leading candidate for patterned media fabrication because of throughput and imprint uniformity [4], and this is reviewed in this paper.

Figure 4 shows a simplified illustration of the UV-nanoimprint process. It is performed at room temperature and pressure. A resist is applied onto the surface by either
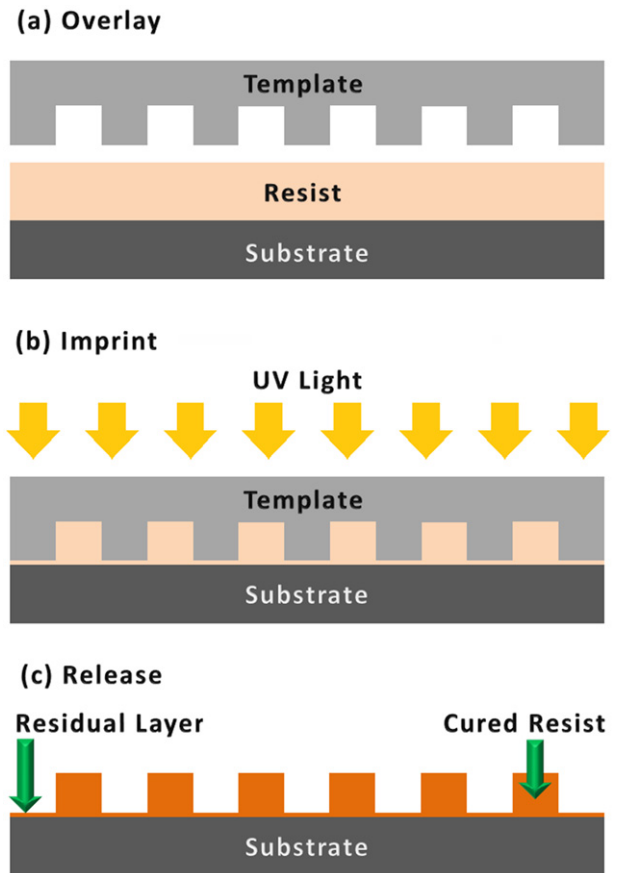
spin-coating a moderate viscosity resist, or locally dispensing a low viscosity resist from an inkjet head [37]. A transparent master template is then pressed into the resist such that the resist fills the pattern in the template. After filling, a UV light source is used to cure the resist. Provided the surface energy of the template and cured resist is low, the template and imprinted substrate are separated [34].

Following a base layer etch to remove the residual resist layer, the imprinted dots can be transferred to magnetic bits. This is discussed in section 5.3.

2.2. Bottom up assembly

Bottom up assembly, and the related term self-assembly [38], involves a molecular system lowering its free energy, and forming organized patterns/structures in the process. As the term self-assembly is used so broadly, it is hard to generalize, but typical advantages over top-down assembly are that smaller feature sizes can be achieved at low cost over a large area. The regular patterns that result could be used in BPM, which requires a regular array of magnetic dots.

One such bottom-up approach to forming BPM is to use block copolymers (BCPs). These materials are known to form periodic patterns when annealed. Using BCPs as

Table 1. Resolution limits and relative costs of the most promising lithographic methods for BPM fabrication.

Technique	Smallest feature size (nm)	Initial investment	Operating cost	Ref
Photo-lithography	19	$$$$	$	[24, 25]
Interference lithography	12.5 (ultimately 6.5)	Technology not proven		[27]
EBL (master only)	8 (2–specialized conditions)	$$	$$	[32]
NIL (replication only)	5	$$$	$	[34, 35]
BCPs	3	$	$	[39, 40]

a method to create BPM is attractive as they are cheap, available commercially and can form structures with a range of periodicities and sizes. However generating uniform patterns over a large area with circular symmetry is not possible using BCPs alone. A solution is to use EBL to direct the self-assembly of the BCP. Combining BCPs with EBL offers the significant benefits of correcting EBL accuracy limitations (pattern rectification) and reducing EBL write times (density multiplication), discussed further in section 4. BCPs will be briefly introduced before sections 4, 6 and 7 take an in-depth look at current approaches to BCP directed self-assembly (DSA).

Table 1 summarizes the various lithographic techniques that can be used to pattern magnetic media along with their associated resolution limits and relative costs.

3. Block copolymers

Since their initial synthesis almost 60 years ago, BCPs have attracted significant interest as self-assembling materials [41]. This interest stems from their ability to self-assemble into patterns at equilibrium with a nanometre sized pattern periodicity. There are various types of BCPs commercially available, for example, triblock and starblock [42–45]. However this review will focus solely on the simplest type of BCP, the diblock, as this has predominantly been used in the fabrication of BPM.

A diblock copolymer consists of two polymer chains (components), labelled in figure 5 as A and B. These two components have different physical properties, so ordinarily they would phase separate like oil and water. However to form the diblock copolymer, they are covalently bonded together, so that this macroscopic phase separation is not possible. Instead to lower the free energy, microscopic phase separation occurs when a BCP film is annealed that results in the formation of a regular pattern [46].

The type of pattern is determined by the composition of the diblock. A key parameter is the volume fraction of each component (where $V_A + V_B = 1$). The values of V_B shown in figure 5 are specific to the BCP polystyrene-polymethylmethacrylate (PS-PMMA). If both components contribute equally to the total volume of the diblock, so that $V_A = V_B = 0.5$, a lamellar pattern is formed (figure 5 lower centre). This lamellar pattern is stable so long as $0.37 < V_B < 0.63$. If $0.33 < V_B < 0.37$ an interconnected gyroid pattern of the B components inside the A matrix is formed (not shown). For $0.21 < V_B < 0.33$ the B component forms hexagonal close packed (hcp) cylinders inside the A matrix. For $V_B < 0.21$ a hcp array of spheres is formed, provided that the film is
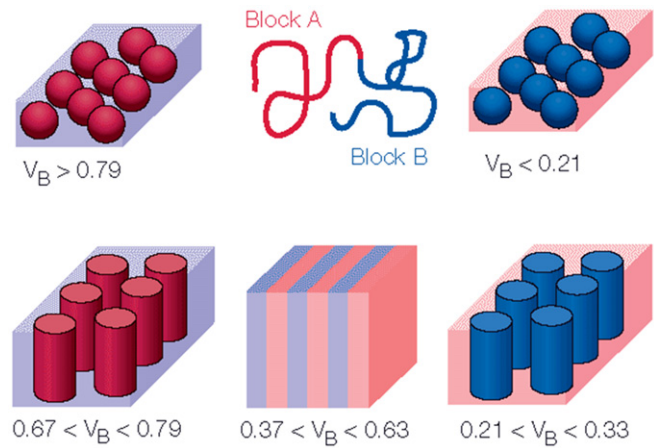

Figure 5. Morphologies formed in a diblock copolymer for various volume fractions, V_B, of component B. Reprinted with permission from [47]. Copyright 2007 PennWell Corporation.

about one period thick to form a monolayer of spheres. Inverse structures are formed for $V_B > 0.63$.

As well as having different physical properties, each component of the BCP will also have different chemical properties. This makes BCPs ideal for lithography, as one component can be selectively removed from a BCP film, leaving, for example, an array of cylinders or spheres that can be transferred into magnetic islands. Details of these processes are given in section 5.

Two key parameters of a BCP are χ and N, where χ is its Flory–Huggins interaction parameter (a measure of the driving force for microscopic phase separation), and N is the degree of polymerization (number of monomer repeats in the chain). The phase separated structure is only stable provided that $\chi N \gg 10$ [48]. To reduce the period of the structures in the BCP film, it's necessary to reduce N, as the period is proportional to $N^{2/3}\chi^{1/6}$ [48], but the $\chi N \gg 10$ condition imposes a limit on the smallest achievable BCP period.

The majority of BCP research for commercial applications has used PS-PMMA, which has multiple properties that make it ideal for lithography [49]. However it has a relatively low χ value of ~0.05 [50]. PS-PMMA periods down to 19 nm have been reported [51], although for defect free phase separation over large areas, 22 nm is currently considered to be the limit [26]. This limits the achievable areal density to approximately 1.5 Tb in^{-2} for hcp circular bits, or 1 Tb in^{-2} for rows of rectangular bits with 1.5 length/width ratio [26]. In the long term it will be necessary to develop processing with alternative BCPs with higher χ values which can enable periods down to 8 nm [52]. However in the short term a lithography technique termed 'line frequency doubling' (discussed in section 5.4)

may be used after the BCP assembly stage to halve the original period of PS-PMMA. If used in both *x* and *y* directions, this has the potential to quadruple the original areal density.

4. Directed self-assembly

The ability of BCPs to self-assemble into ordered patterns without defects is one of their main advantages for their use in BPM formation. However these ordered patterns do not extend over a large area, as instead boundaries form between small areas of ordered patterns. Therefore BCPs cannot, on their own, be a useful tool for the production of BPM [5], [46]. Instead, by combining 'top-down' templating with the 'bottom-up' self-assembly of BCPs, the ordered pattern area can be made arbitrarily large [53–55]. Placement jitter, feature size distribution, and pattern registration can also be improved by this DSA approach [56].

Many techniques have been investigated to control the positioning of BCPs. These include temperature gradients [57], electric fields [58], shear fields [59] and directional solidification [60]. An earlier review by Darling [61] comprehensively covers the various techniques. Whereas all these techniques provide orientational ordering, only graphoepitaxy and chemoepitaxy provide additional control over translational ordering and feature registration [62].

Graphoepitaxy (explored in section 6) uses physical control—by patterning physical features into the substrate surface, a BCP film will self-assemble around, or within these features. Chemoepitaxy (explored in section 7) uses chemical control—by patterning chemical regions onto the substrate surface, it becomes thermodynamically more favourable for one of the BCP components to assemble on top of the chemically modified region, allowing component position to be directed.

The use of these epitaxial techniques confers two advantages. The first is 'density multiplication'. Rather than patterning the whole substrate surface at a density equivalent to the BCP period, a sparse pattern can be written instead, reducing EBL write times. Provided the pattern is not too sparse, it will have the effect of directing the self-assembly of BCPs, which 'fill in the gaps'. A density multiplication factor can be obtained in these experiments—for example, if for every four resulting magnetic dots, only one of them was directly patterned by EBL, this is a density multiplication factor of 4, and corresponds to a 75% reduction in EBL write time.

The second advantage is termed 'pattern rectification'. For example with trenches used in graphoepitaxy, EBL does not create perfect edges, resulting in line edge roughness (LER). BCP components adjacent to the trench walls will follow the LER, but BCPs further from the walls have a more uniform placement due to their strong lateral ordering. In the case of chemically patterned regions (chemoepitaxy), the BCP component position is not solely influenced by the placement of the underlying chemical region, but is also influenced by the placement of surrounding components. Therefore small deviations in chemical region placement caused by EBL accuracy limitations tend to get averaged out, with the overlying BCP film having a tighter placement distribution.
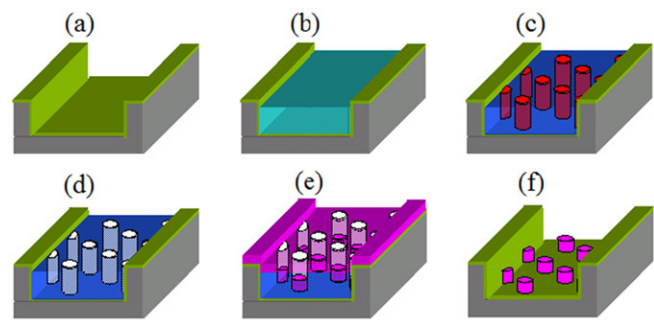

Figure 6. Formation of magnetic arrays by an additive process. (*a*) The substrate in this example has had a trench cut into it. (*b*) PS-PMMA is spin-coated onto the substrate. (*c*) Annealing of PS-PMMA forms ordered BCP components. (*d*) Removal of PMMA blocks by etching. (*e*) Deposition of magnetic cobalt metal. (*f*) Lift-off of PS matrix removes unwanted metal, leaving an array of Co dots. Reprinted with permission from [66]. Copyright 2005 Institute of Physics.

Once the BCP components are arranged into the required pattern, a technique is required to transfer the pattern into magnetic dots. These techniques are introduced in the next section, so that the link between BCPs and the final magnetic arrays can be demonstrated. Sections 6 and 7 then discuss in greater detail the grapho- or chemoepitaxy methods used to arrange BCP components into the required pattern.

5. Creating magnetic arrays from BCPs

Once the BCP components are arranged in a suitable pattern, transfer processing is required to convert the components into magnetic dots. Section 5.1 explains how this can be carried out directly.

The downside of direct conversion is that the BCP DSA process will have produced only one magnetic array. As BCP DSA is a time consuming process, mass production of HDDs will require many magnetic arrays (disks) to be produced from a single original sample of ordered BCP. This will be achieved by converting the BCP components into a topographic template, which can be used as the master imprint template in NIL (section 9). Section 5.2 explores the processing required for this conversion into a NIL template, and section 5.3 discusses the subsequent processing required to convert imprinted substrates into magnetic dot arrays.

5.1. Direct conversion to a magnetic array

A magnetic array can be made directly from BCP components using either an additive or subtractive process, or by etching the underlying substrate.

5.1.1. Additive film processing. Additive processing is demonstrated in figure 6 with the BCP PS-PMMA. On the substrate in figure 6(*a*) (here shown with a trench cut into the substrate) PS-PMMA is spin-coated (figure 6(*b*)). Thermal or solvent annealing is used to aid micro-phase separation, so that BCP ordering occurs, as shown in figure 6(*c*). Etching of one of the components then takes place. For PS-PMMA, the

J. Phys. D: Appl. Phys. **46** (2013) 503001

Topical Review

PMMA components can be selectively removed by exposure to UV radiation followed by an acetic acid rinse [63] as used in this example, or by oxygen plasma treatment [64]. The plasma etch contrast between the components is only about 2, which is lower than the wet etching process, but it better preserves the structure and dimension of the PS matrix without sidewall collapse or excessive roughness [65]. Etching of the PMMA blocks is shown in figure 6(*d*). A film of the magnetic material is then deposited as shown in figure 6(*e*). The film that deposits in the empty cylinders makes contact with the substrate, whereas the remainder sits on the PS matrix. Finally lift-off is carried out by removing the PS matrix, which lifts off the magnetic material on top, leaving magnetic arrays in the original PMMA pattern, as shown in figure 6(*f*).

5.1.2. Subtractive film processing. Subtractive processing allows the magnetic properties of the thin film and the pattern transfer process to be optimized independently. In a subtractive process, the magnetic material is deposited first, followed by spin-coating of the BCP film. After annealing, one of the BCP components can be etched, exposing the magnetic material underneath in the pattern of the removed component.

An example of subtractive patterning was performed by Cheng *et al* [67] to pattern a Co film. Ideally one component of the BCP could be used directly as an etch mask for the Co, but in practice this is not possible. A silica layer is used in this example to promote good wetting of the substrate by the BCP. Co cannot be etched by a RIE process because it does not form volatile products, and instead requires physical sputtering with Ar$^+$ ions (known as ion beam etching or ion milling). A hard mask of W is required for this process. Onto this stack of silica, tungsten and cobalt, a thin film of the BCP polystyrene-polyferrocenylsilane (PS-PFS) was spun and then annealed. Oxygen plasma was used to etch the PS, followed by patterning of the silica using CHF$_3$ RIE. Next a CF$_4$ and O$_2$ RIE was used to transfer the pattern into the tungsten layer before ion milling was used to generate the final pattern of cobalt islands. This process is shown in figure 7.

5.1.3. Substrate etching. An alternative technique is to etch the underlying Si or glass substrate to form pillars, as described in section 5.2. Rather than using it as an imprint template, a magnetic film can be sputtered directly on top of the Si structures as shown in figure 8. As the film is added on top, it can be classed as an additive process, although it differs from the process described in section 5.1.1 as the film that is deposited in the trenches between the pillars is allowed to remain, rather than being removed by a lift-off process.

Hu *et al* [68] defined that the minimum trench depth must exceed the film thickness in order to preclude direct contact between the magnetic layers on pillar tops and trench bottoms. These authors reported a compromise design of a trench depth of 24 nm and film thickness 10 nm. Hellwig *et al* [23] used a pillar height of 53 nm with a film thickness of 14 nm to ensure exchange decoupling of island and trench material, such that the islands reverse as individual units. Care must be taken when analysing data from experiments on these arrays to be sure that the signals of interest are coming from islands rather
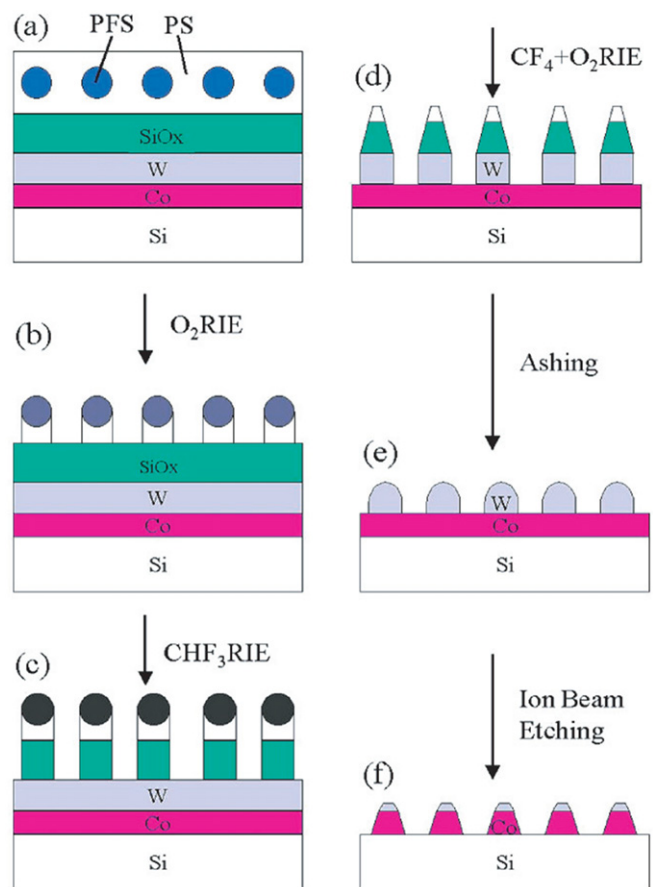

Figure 7. Subtractive method of forming BPM. (*a*) The BCP on a multilayer of thin films of silica, W, Co, with Si as the substrate. (*b*) O$_2$ plasma used to selectively etch the PS. (*c*) Patterning of the silica by CHF$_3$ RIE. (*d*) CF$_4$ + O$_2$ RIE used to pattern the W layer. (*e*) High pressure CHF$_3$ RIE is used to remove the silica and residual polymer. (*f*) Ion milling generates the desired Co array. Reprinted with permission from [67]. Copyright 2001 John Wiley & Sons, Inc.
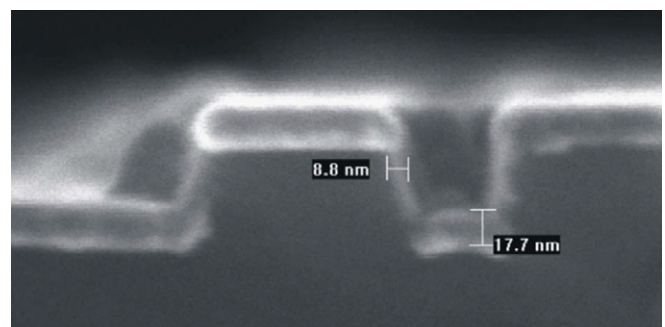

Figure 8. SEM image of 100 nm wide lines separated by 50 nm trenches covered by a multilayer film where the structure is SiO$_2$/50 Å Pd/(3 Å Co/8 Å Pd)$_{10}$/10 Å Pd. Reprinted with permission from [68]. Copyright 2004, AIP Publishing LLC.

than trench material. In practice this is often straightforward as they have quite different switching fields.

5.2. Conversion to a master imprint template

A working template will consist of patterned quartz (SiO$_2$), whereas submaster templates (used as intermediate NIL

templates, described further in section 7.2) will consist of patterned Si. Suitable transfer processes are required to transfer BCP patterns into these materials. Wan *et al* [69] have reported how this can be achieved. PS-PMMA was spin-coated, and PMMA was selectively removed. Cr was then deposited, and a lift-off process left Cr as a mask in the original PMMA locations. Fluorine-based RIE was then used to etch the underlying substrate in both cases (quartz and Si) leaving topographic pillars. A related process that deposits spin-on glass following Cr deposition has been reported to result in improved transfer at sub-27 nm period [26].

5.2.1. Sequential infiltration synthesis. BCP films are thin and their components typically erode quickly in a plasma, meaning the masking BCP film is completely removed before features with sufficient depth are transferred into an underlying substrate [70]. For this reason, an alternative hard mask layer is required, for example Cr formed by lift-off as described in section 5.2 for forming topographical features in a quartz or Si substrate. The usage of hard mask layers adds complexity to the process, and requires materials satisfying several requirements which can be hard to find [71].

Recently a new process termed sequential infiltration synthesis (SIS) [72, 73] has been proposed to remove the need for a hard mask layer, and allow a BCP pattern to be transferred directly into the underlying substrate. SIS makes use of the more established technique of atomic layer deposition (ALD) to infiltrate a polymer with inorganic materials. The application of SIS to the BCP PS-PMMA is described as follows: a PS-PMMA film is placed into an evacuated ALD reactor and first exposed to gas-phase trimethyl-aluminium (TMA). The TMA molecules are able to diffuse through the film where they selectively react with the carbonyl groups on the PMMA chains. The chamber is then evacuated before being purged with N_2 to remove unreacted TMA and byproducts. Water vapour is then introduced to the chamber where it reacts with the TMA molecules bound to the PMMA chains, forming Al_2O_3. Subsequent SIS cycles can be used to increase the amount of Al_2O_3 within the PMMA components by growing material from aluminium oxide seeds nucleated during the first cycle. The SIS-modified PMMA components are resistant to a variety of plasma chemistries, which can allow pattern transfer into diverse substrate materials. The full process as demonstrated by Tseng *et al* [70] is shown in figure 9. The PS-PMMA has SIS applied to it to form Al_2O_3 within the PMMA components (figure 9(*a*)). Oxygen plasma is then used to remove the PS component (figure 9(*b*)). Breakthrough of the thin surface alumina layer is achieved using BCl_3-based plasma (figure 9(*c*)). The underlying substrate is then etched using an appropriate plasma chemistry (figure 9(*d*)). Finally the SIS-modified resist can be removed by wet etching (figure 9(*e*)), for example in a bath of tetra-methyl-ammonium-hydroxide [74], leaving topographic pillars (figure 9(*f*)).

Ruiz *et al* [75] combined DSA of 41 and 27 nm period lamellar PS-PMMA with SIS to etch 20 nm deep into a Si substrate. They found that three TMA/water exposure cycles gave the best tradeoff for forming a continuous hard
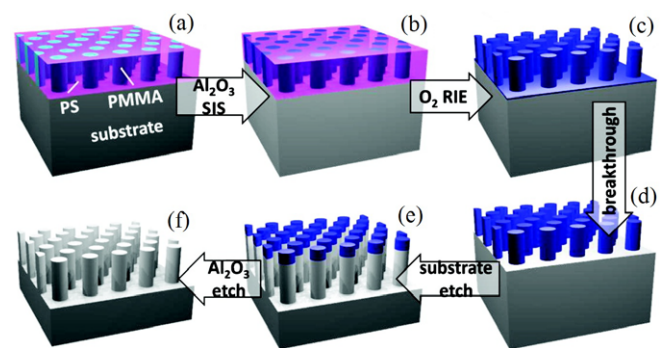

Figure 9. Substrate patterning using SIS. (*a*) SIS is used to infiltrate alumina into PMMA components. (*b*) Oxygen plasma removes the unreacted PS components. (*c*) Breakthrough of thin surface alumina layer using BCl_3-based plasma. (*d*) Etch into substrate using the appropriate plasma chemistry. (*e*) Removal of mask. (*f*) End result of topographic pillars. Adapted with permission from [70]. Copyright 2011 American Chemical Society.

mask pattern without generating excessive pattern distortion. The resulting sidewall etch profiles of the Si structures were sufficiently vertical, with a flat top surface, and LER that meets the BPM specification. Occasional defects such as broken lines and pattern bridging resulted due to the level of aluminium oxide infiltration varying, meaning that further work is required in finding conditions that mitigate this.

5.3. From imprinted resist to BPM platter

Once the master template is fabricated it can imprint many substrates. Resist is dispensed onto a Si substrate, and the master template is used to imprint the resist in the manner described in section 2.1.1. Following a base layer etch to remove the residual layer, there are two possible methods to transfer the imprinted dots into magnetic bits.

In an additive process, substrate pillars are created from the imprinted resist using the same methods as in section 5.2. The magnetic film is then deposited on top of these pillars, leaving a result similar to figure 8. It also shares the same issues of magnetic noise from the magnetic material in the trenches between the bits [76], although the spacing difference between the read head and the magnetic material reduces this effect.

Instead, a subtractive process is likely to be favoured. Here, the magnetic film is deposited first before dispensing resist and imprinting. The underlying magnetic film is then etched. Etching can be done using a carbon hard mask and ion milling or ion implantation [52]. Albrecht *et al* [52] achieved this using a thin (6–8 nm) CoCrPt film, resulting in magnetic islands at 1 Tb in^{-2}. These islands had excellent thermal stability in the range of $K_u V / k_B T = 150$ or higher, suggesting good extendibility for recording at higher densities.

5.4. Line frequency doubling

An additional lithographic process can be carried out after BCP film deposition in order to increase the resulting areal density. This process is termed line frequency doubling, of which there are two main types—double lithographic patterning (DLP) [77], and spacer defined double patterning (SDP) [78].
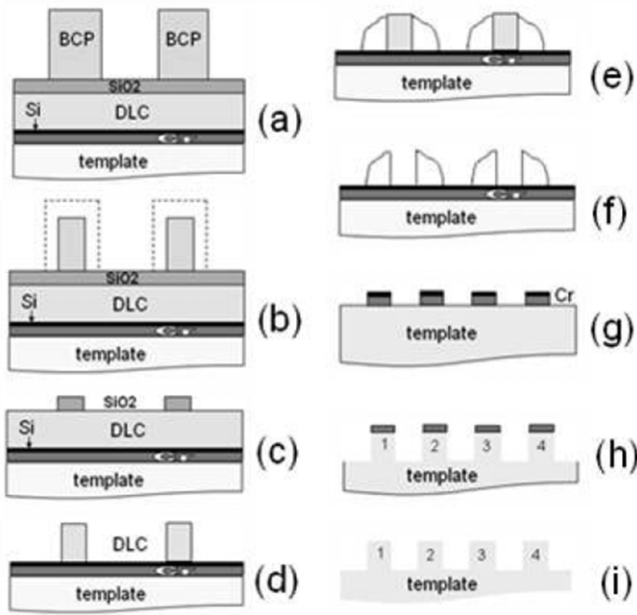
Figure 10. Line frequency doubling. (*a*) Initial BCP pattern.
(*b*) BCP trimming. (*c*) Pattern transfer to first SiO$_x$ hardmask.
(*d*) Pattern transfer to sacrificial carbon layer. (*e*) Spacer deposition
and anisotropic etch back. (*f*) Removal of sacrificial carbon
between spacers. (*g*) Pattern transfer from spacers to Cr hardmask.
(*h*) Si substrate etch. (*i*) Wet etching of remaining Cr. Reprinted
with permission from [49]. Copyright 2012 Society of Photo
Optical Instrumentation Engineers.

Patel *et al* [49] have recently demonstrated the use of SDP
following lamellar PS-PMMA phase separation in order to
achieve lines with a full period of 13.5 nm—half the original
27 nm period of the PS-PMMA. Figure 10 illustrates their SDP
process. The PMMA blocks have been removed, leaving PS
blocks on the surface (figure 10(*a*)). The width of the PS blocks
are trimmed to become roughly 1/4 of the starting period
with oxygen based plasma (figure 10(*b*)). Fluorine based
plasma transfers them into the SiO$_x$ cap layer (figure 10(*c*)).
Oxygen based plasma then transfers them into the sacrificial
carbon layer, leaving carbon pillars (figure 10(*d*)). Next
a spacer material is deposited which surrounds the pillars
(figure 10(*e*)). The carbon pillars are removed with RIE,
leaving spacer pillars at a density double that of the original
PS blocks (figure 10(*f*)). Cl-based RIE transfers them into the
underlying Cr hardmask layer (figure 10(*g*)), and a fluorine-
based RIE transfers them into the Si template (figure 10(*h*)).
Any remaining Cr hardmask is removed with wet chrome
etchant, leaving Si pillars (figure 10(*i*)).

Although this is a long sequence of steps, it would only
have to be carried out when producing a master template.
This could potentially be used with the lithographic techniques
described in section 7.2 to halve the period in both *x* and *y*
directions.

6. Graphoepitaxy

Graphoepitaxy is a technique where physical patterns are
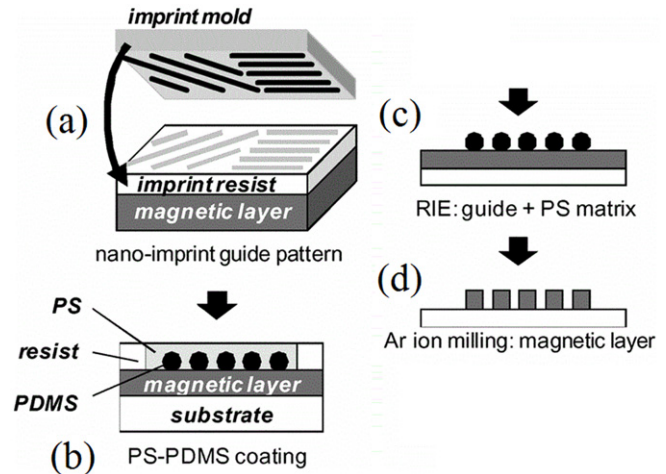written into a substrate in order to direct self-assembly of

Figure 11. Simplified process flow showing the formation of tracks
of BPM via graphoepitaxy. (*a*) A template is used to form trenches
in a resist. (*b*) A BCP is then deposited so that it fills the trenches,
and forms an ordered pattern when annealed. (*c*) The trench walls
and PS component can subsequently be removed, and (*d*) the BCP is
transferred into the underlying magnetic layer. Adapted with
permission from [81]. Copyright 2013 IEEE.

BCPs. Any arbitrary pattern can be written and filled with a
BCP, and in section 8 we show that this is advantageous when
creating servo patterns with shapes that are not amenable to
chemoepitaxy DSA.

6.1. Templates with deep topographical features

Patterning deep topographical features into a template makes it
relatively easy to control where the BCP is located, as it 'fills
in the gaps'. This will be explored first before sections 6.2
and 6.3 look at advantages of using shallower features.

6.1.1. Topographical trenches. To date the most widely
researched graphoepitaxy patterns have been grooves or
trenches [79]. Templates with trenches cut into the substrate
can be formed using EBL followed by etching. A BCP is then
deposited so that it fills the trenches, and annealing results in
ordered pattern formation. An alternative method is to use a
NIL template to pattern trenches into a resist rather than the
substrate [80]. A simplified schematic of this can be seen
in figure 11(*a*), followed by filling the trench with a BCP
and annealing (figure 11(*b*)), and transfer into the underlying
magnetic layer (figures 11(*c*) and (*d*)). It can be seen that the
trench walls are removed, so the resulting BPM consists of
tracks of magnetic islands on a flat surface.

In an early demonstration of graphoepitaxy, Segalman
et al [82] patterned trenches ranging from 1 to 10 μm width into
a SiO$_2$ layer using photolithography. Polystyrene-block-poly-
2-vinylpyridine (PS-P2VP) self-assembled within the trenches
into spherical components, parallel to the trench pattern, and
demonstrated long-range order. However this process has
limitations, because beyond a certain trench width, ordering
of the BCP components diminishes.

To demonstrate this, Cheng *et al* [79] patterned 80 nm
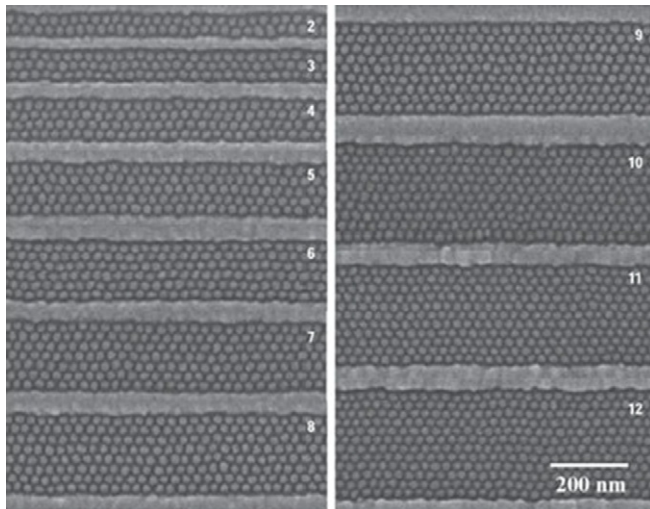deep trenches into a SiO$_2$ substrate using EBL. The trench

Figure 12. Plan-view scanning electron micrograph of ordered arrays of PFS components with $N = 2$ to 12 rows. Reprinted by permission from Macmillan Publishers Ltd: Nature Materials [79], copyright 2004.
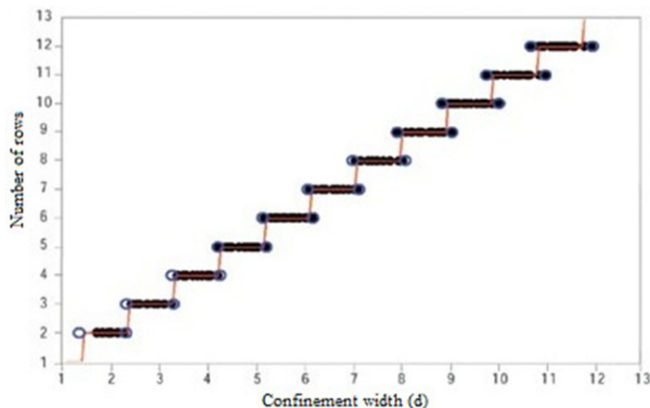

Figure 13. This graph shows the number of rows of BCP that can fit into a trench of a particular width. As width increases, there are increasingly large width regions where N or $N + 1$ rows are stable. The confinement width is expressed in terms of d, the equilibrium row spacing, which is 24.8 nm in this polymer. Reprinted by permission from Macmillan Publishers Ltd: Nature Materials [79], copyright 2004.

widths varied from 60 to 500 nm, which can accommodate 2–19 parallel rows of the spherical components of PS-PFS. Figure 12 shows the ordered arrays of the PFS spheres (after removal of the PS matrix) arranged within the increasing trench widths in the substrate. Order remains until there are more than 12 rows of PFS spheres in a trench. Above this the BCP may form either N or $N + 1$ rows. This probability is represent graphically in figure 13 and leads to a breakdown in long range order. Because a certain minimum trench width is required for ordering to occur, a significant area of the surface is taken up by the gaps between the trenches. Therefore, although this method is attractive due to its simplicity, it has a downside of compromising the storage space. In addition, trenches only provide 1D guidance, and do not prevent translational wander over long distances of the BCP pattern in the downtrack direction.
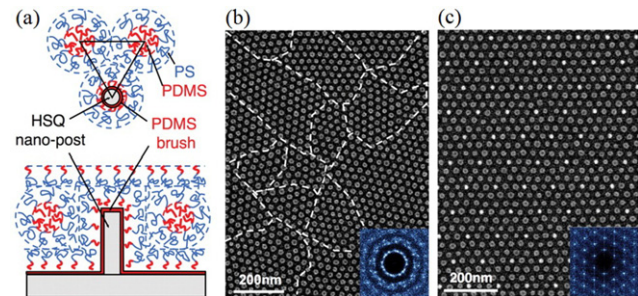

Figure 14. (*a*) Top-down and side-view schematic of PS-PDMS self-assembling onto the template directed by the chemically functionalized topographical posts. (*b*) SEM of the formation of small area ordered regions of PS-PDMS without the use of graphoepitaxy. (*c*) SEM of long range order obtained by using topographical posts to create a sparse template. Reprinted from [83] with permission from AAAS.

6.1.2. Topographical posts. A sparse pattern of topographical posts on the substrate surface can be used to guide the self-assembly of BCPs. Each post is designed to act as a surrogate spherical or cylindrical component of the minor component of the BCP, and be nearly chemically and physically indistinguishable from the BCP entity for which it substitutes [83]. Therefore it is necessary to chemically functionalize the posts. This is typically done using a random copolymer such as polydimethylsiloxane (PDMS) homopolymer brush [83, 84] or hydroxyl-terminated PS-PMMA [66, 85].

It should be noted that if posts are used to template the BCP, and the components are then directly converted into magnetic dots, the posts will occupy positions where magnetic dots would otherwise be located. This means the density multiplication factor is less than theoretically predicted and would also cause issues in a practical BPM HDD as magnetic dots would not be present at all the locations where data could be recorded. However, if the posts and BCP components can be converted into topographically identical features and used as a master template in NIL, the density multiplication factor and recording integrity would be restored.

Bita *et al* [83] used scanning EBL to create posts of a comparable size to the spherical component of PS-PDMS. Figure 14(*a*) illustrates the topographic and chemical design of the posts used. The template was functionalized with a short PDMS homopolymer brush, and a post substitutes for a PDMS sphere in the close-packed array. Figure 14(*b*) illustrates the small regions of order that result without templating, whereas figure 14(*c*) demonstrates that long range order is achieved when using a sparse 2D lattice, resulting in a density multiplication factor of 9.

In a similar fashion to Cheng *et al* [79] (figure 12), this group investigated how sparse it is possible to make the template pattern while maintaining long-range order. They demonstrated BCP patterns ordered by posts with density multiplication factors as high as 20. For even higher density multiplication, a rectangular guiding pattern is reported to be superior to a hexagonal guiding pattern [86]. In a theoretical study, Tang and Ma [87] explored the highest density multiplication factor that could be achieved using a
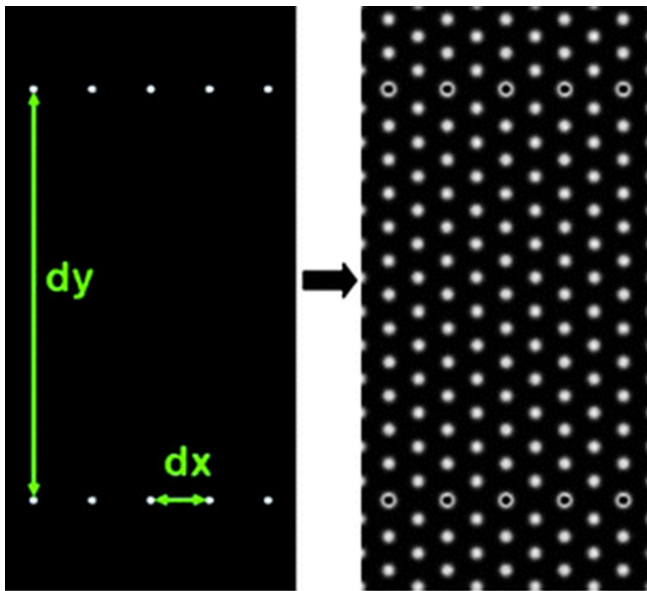
Figure 15. An illustration of a rectangular lattice template to induce the final equilibrium morphology of the BCP components. Reprinted from [87] with permission of The Royal Society of Chemistry.

Figure 16. Schematic illustration of the strategy used for generating the perpendicular cylinder pattern on highly oriented crystalline facets on a single crystal surface. (*a*) The M-plane sapphire was annealed to form sawtooth patterns. (*b*) The flat surface of the M-plane sapphire reconstructs into facets with the ($\bar{1}$ 1 0 1) and (1 $\bar{1}$ 0 2) planes on opposite edges. (*c*) Smooth PS-PEO thin films were spin-coated onto these surfaces. (*d*) Solvent annealing produced highly ordered perpendicular cylinders. Adapted from [89] with permission from AAAS.

rectangular lattice of cylindrical posts, illustrated in figure 15. Using a suitable BCP they predict that the spatial frequency in the x direction can be multiplied by a factor of 2, and in the y direction by a factor of 17, resulting in a density multiplication factor of 34.

The high density multiplication factors achieved by the use of posts would enable a significant reduction in EBL write time. On the other hand, placement deviation tends to increase as guiding patterns are made more sparse, so there is a limit to how far it is wise to go. An array of posts provides 2D guidance, rather than just 1D guidance as with trenches. However, the presence of non-magnetic posts along a track of magnetic islands would complicate BPM operation. This could be avoided if both the BCP components and posts could be transferred to topographically identical features in a NIL template, although to our knowledge this has not yet been demonstrated.

6.2. Shallow topographic features

One of the main issues with using deep trenches to direct the self-assembly of BCPs is that their depths are larger than the centre-to-centre distance between the BCP components. This results in BCP being restricted to trenches, and would compromise storage space in a BPM HDD. Instead, if shallow features are used, BCP ordering can be achieved over macroscopic length scales [88].

Park *et al* [89] demonstrated this concept by using a reconstructed crystal surface to direct ordering, as shown in figure 16. Large, defect-free single-crystalline wafers of silicon or sapphire were used as the substrate. The single crystals were cut along specific crystallographic planes, which upon thermal annealing generated a sawtooth topography over the entire substrate surface as the surface reconstructs and crystal facets form.
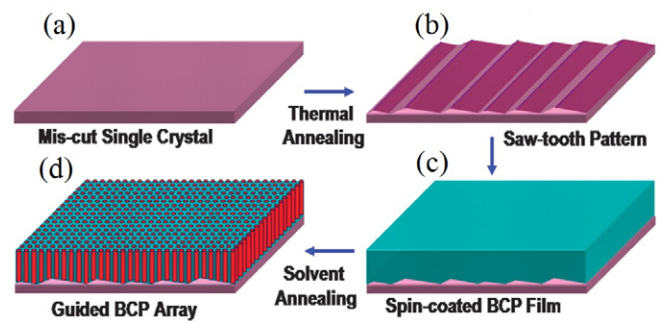
A range of polystyrene-polyethylene oxide (PS-PEO) BCPs with different molecular weights were investigated. The self-assembly of BCPs was guided by the small amplitude ridges of the facets rather than by a confinement effect between facets. By optimizing the film thickness, they were able to order the cylinders perpendicular to the surface over the $25 \times 25\,\mu m^2$ area scanned by AFM. This technique was demonstrated for areal densities from 0.74 to 10.5 Tb in^{-2}. Interestingly it was also observed that as the BCP period decreased, the orientation and translational order improved. These results were found to be reproducible when using alternative BCPs (PS-P2VP and PS-P4VP).

On any single-crystalline substrate, there will be defects such as dislocations in the facets on the reconstructed surface. However, it was shown that the BCP self-assembly exhibits pattern rectification, meaning that BCP ordering is not affected by the underlying defects. To demonstrate this, the authors took an AFM image of an area of the ordered BCP film. They then removed the film by rinsing the substrate in benzene and took an AFM image of the cleaned substrate at the same location. This revealed many dislocations in the surface which had not been apparent in the BCP film, showing that the BCP self-assembly overrides these defects.

Whilst 10.5 Tb in^{-2} is a very high areal density at which to have demonstrated long range order, it should be noted that this technique does not create the circular symmetry required in practical BPM. In addition the BCP period is generally not commensurate with the underlying sawtooth period (which has randomly occurring steps, with just an average period being roughly constant over long distances), meaning that precise guidance of the BCP component placement does not occur.

6.3. Circular topographies

While there has been much research and progress into reducing feature size and increasing long range order of BCPs, most methods create patterns of parallel lines or arrays of dots. However, for this development to be utilized in rotating disk
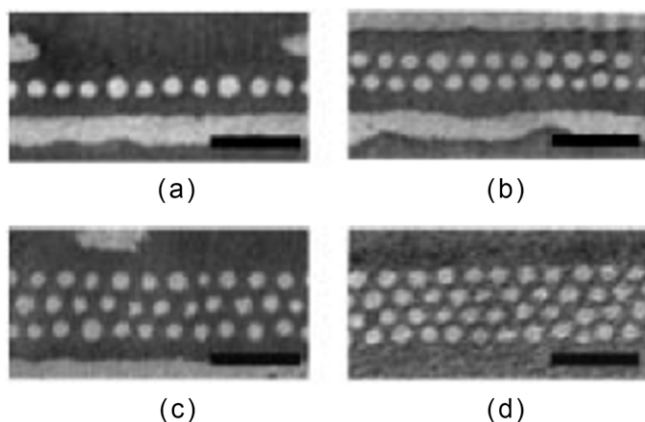
Figure 17. AFM of the spherical components of PS-PMMA formed in trench widths of (*a*) 60, (*b*) 150, (*c*) 200 and (*d*) 250 nm. The scale bar indicates 300 nm. At this scale, the curvature of the trenches is not apparent. Reprinted with permission from [64]. Copyright 2002 IEEE.

systems, magnetic arrays must be generated with circular symmetry [88, 90].

Naito *et al* [64] first demonstrated the possibility of creating circular arrays of BPM with the use of trenches. The BCP PS-PMMA, was introduced onto the template with 60, 100, 150, 200 and 250 nm trench widths, all 110 nm deep. The trenches extended around a circular 2.5 inch HDD glass platter. The BCP was then annealed and PMMA spheres with 40 nm diameter formed within the trenches. AFM images, shown in figure 17, demonstrate that order is maintained as trench width increases. Fluctuations in the size of the spheres can be seen showing that optimization of the annealing process is required, and LER of the trenches causes deviations in the sphere positions. However, this result shows that long range BCP ordering with circular symmetry can be achieved.

Hong *et al* [88] also demonstrated the successful synthesis of circular arrays by using shallow circular trenches. They generated three different patterns with varying trench widths (29, 31 and 34 nm) and respective distance between the trenches (80, 99 and 121 nm). The BCP PS-PEO with a 32.3 nm period cylindrical morphology was introduced to each of these patterns and annealed.

The trenches had a shallow depth of only 8 nm, much smaller than previously reported [64, 90]. This means that BCP ordering was not restricted to isolated trenches as the depth was shallower than the centre-to-centre distance between the BCP components. Hence, a thin flat film formed over a large area. In this experiment, solvent annealing caused the cylinders to lie parallel to the surface. Of the three templates generated, only the middle, M, pattern (trench width of 31 nm and distance between trenches of 99 nm) showed a highly ordered BCP morphology. This middle region of trenches extended around a circle of radius 18 mm, demonstrating long range order. The other two templates with the smallest and largest topography (trench width 29 and 34 nm and respective distance between trenches of 80 and 121 nm) showed fingerprint type patterns, indicating that the circular trenches did not direct the self-assembly of the BCP as required. This is understandable as only the trenches with 99 nm period are close to being an
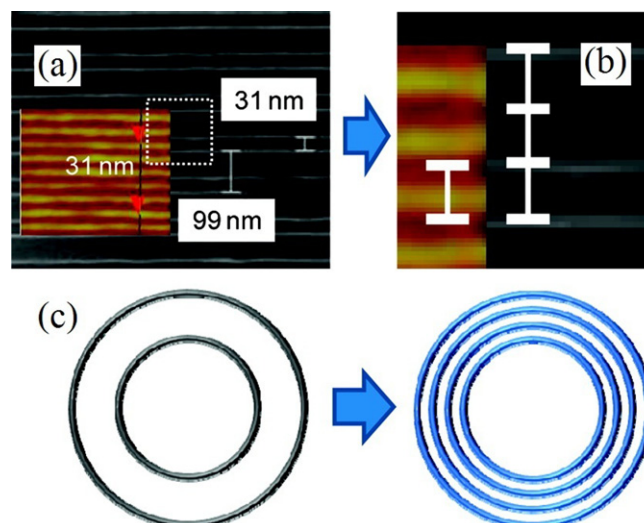

Figure 18. (*a*) Superposition of an AFM image of the PS-PEO lamellae with an SEM image of the trenches. (*b*) Magnification of the white dotted box in (*a*). (*c*) Schematic diagram representing 3× density multiplication of circular patterns. Reprinted with permission from [88]. Copyright 2011 American Chemical Society.
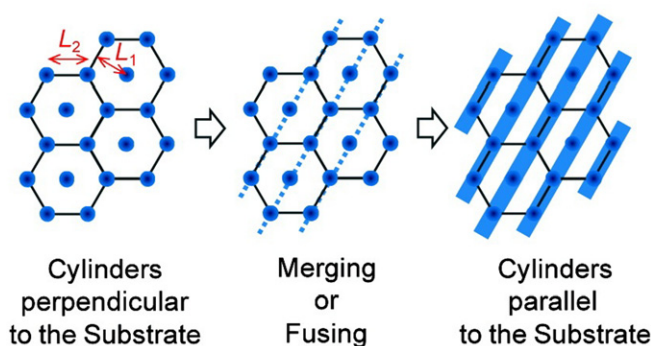

Figure 19. Graphical representation of the transformation of PEO cylinders from perpendicular to parallel orientation as solvent annealing proceeds. Reprinted with permission from [88]. Copyright 2011 American Chemical Society.

integer multiple of the BCP period of 32.3 nm. This 3× density multiplication can be seen in figure 18 with the superposition of BCP and trench images.

The period of the BCP could potentially be reduced as long as the commensurability with the trenches is maintained. Repetition of this method was performed using the BCP PS-P2VP to demonstrate its general applicability.

A graphical representation of the cylinders changing from perpendicular to parallel orientation is shown in figure 19. By analysing AFM images, the authors demonstrated that the cylinders orientate to lie within the trenches. The resulting lamellar-like pattern is not directly useful in the formation of BPM, and could only be directly used to form less promising discrete track media. However, if the parallel cylinder template was used as a submaster template in NIL along with another submaster consisting of radial lines, concentric circular tracks of BPM could be achieved. This is explored further in section 7.2.

Whilst the use of shallow trenches has the advantage of not compromising storage space, a problem is the resulting height

variations. For the previous example of parallel cylinders in trenches with $3\times$ density multiplication, the lines of cylinders within the trenches would presumably be 8 nm lower than the cylinders outside of the trenches. The rms surface roughness of recording media is required to be no larger than 0.3 nm [91], so existing designs could not operate if the resulting tracks of magnetic islands had a 8 nm height difference.

7. Chemoepitaxy

The second approach to directing the long range order of BCPs for BPM applications is called chemoepitaxy or chemical prepatterning. In this technique the surface is patterned to have two different chemical environments. Epitaxy occurs when the BCP is spin-coated on top, as each component of the BCP is attracted to one of the two chemically different regions. This weak directing influence is enough to cause ordered pattern formation to occur over an arbitrarily large area, rather than the sub-micron sized ordering that typically occurs. An early demonstration of this technique was given by Kim *et al* [92] where photoresist was patterned into alternating lines and spaces using EUV-IL, and then exposed to x-rays, causing the exposed stripes of the underlying self-assembled monolayer to become polar. The photoresist was then removed, and lamellar PS-PMMA was spin-coated on top with a period equal to the stripes, so that each component was attracted to one of the two regions. More recent work reviewed in this section uses EBL to pattern the resist, and chemical etching techniques to generate chemical contrast, but the principle is the same. As with graphoepitaxy various shapes can be created, making it a useful technique not only for BPM creation but for nanolithography in general [93, 94].

7.1. Chemical prepatterning of cylinder arrays

BPM places stringent requirements on bit size and spacing. For this reason cylinder-forming BCP films are preferred over sphere-forming BCP films, as film thickness can be adjusted to optimize BCP annealing [94]. In addition, the low height/width aspect ratio of spheres, plus the residue of the majority component beneath the spheres, makes them less suitable as an etch mask for subsequent pattern transfer [95]. The following section reviews the formation of BCP cylinder arrays using chemoepitaxy.

7.1.1. Pattern rectification and density multiplication.
As introduced in section 4, an additional benefit of DSA is pattern rectification. The ability of BCPs to rectify a chemical prepattern is highly advantageous as it allows the BCP annealing process to overcome inconsistencies in the e-beam patterned substrate, thus allowing higher e-beam currents and faster resists to be used.

An example of pattern rectification was demonstrated by Ruiz *et al* [62]. Figure 20 shows the patterning process the authors used to create chemical contrast. A brush of hydroxyl-terminated polystyrene (PS-OH) was deposited on a SiO_x substrate. E-beam resist was then deposited on top, and EBL was used to write a hexagonal pattern over a total area of
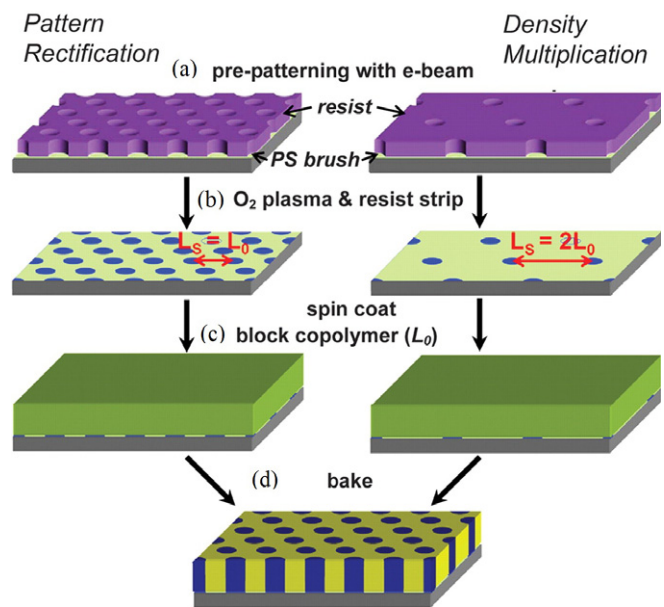

Figure 20. Chemoepitaxy process used to create an ordered hexagonal array of PS-PMMA. Reprinted from [62] with permission from AAAS.

$100 \times 100 \,\mu m^2$ (figure 20(a)). The hexagonal pattern lattice constant L_s was chosen such that $L_s = nL_0$ with $n = 1, 2$, where L_0 is the BCP period. A brief dose of oxygen plasma was used to generate chemical contrast before the remaining resist was removed (figure 20(b)). The BCP PS-PMMA was then spin-coated (figure 20(c)) and annealed in a vacuum to give the desired hexagonal array (figure 20(d)). The PMMA component interacts preferentially with the regions which were exposed to the O_2 etch, while the PS component has a slight preference for the PS-OH. The PMMA component was then selectively removed using UV irradiation and acetic acid etching, leaving a matrix of PS surrounding holes where PMMA was removed.

By analysing approximately 15 000 dots of both the developed e-beam resist and corresponding BCP patterns it was apparent that the BCP patterns had much narrower placement and size distributions than the e-beam prepatterns. The pattern rectification is also easily visualized in the plan-view SEM images of the patterned e-beam resist and matching BCP patterns, shown in figure 21. A comparison of figures 21(a) and (c) shows that the latter contains far less variation in pattern parameters (spacing and size) than the former.

In addition, when L_S was equal to twice the BCP lattice constant ($L_S = 2L_0 = 78$ nm), the PMMA component interacted with the prepatterned sites as well as forming perpendicular cylinders in the sites between the e-beam patterning. This multiplies the density of pattern features by a factor of four (two in each direction), as can be seen by comparing figures 21(b) and (d). The tolerance of this commensurability is approximately $\pm 0.1\,L_0$ showing that this density multiplication is sensitive to the locations of the 'sparse' pattern. Long range order ($100 \times 100 \,\mu m^2$) is, however, preserved throughout the prepatterned area with a defect density of $<10^{-4}$ for patterns with $L_S = 27, 39$ and 78 nm and $<10^{-3}$ for patterns with $L_S = 54$ nm, below the
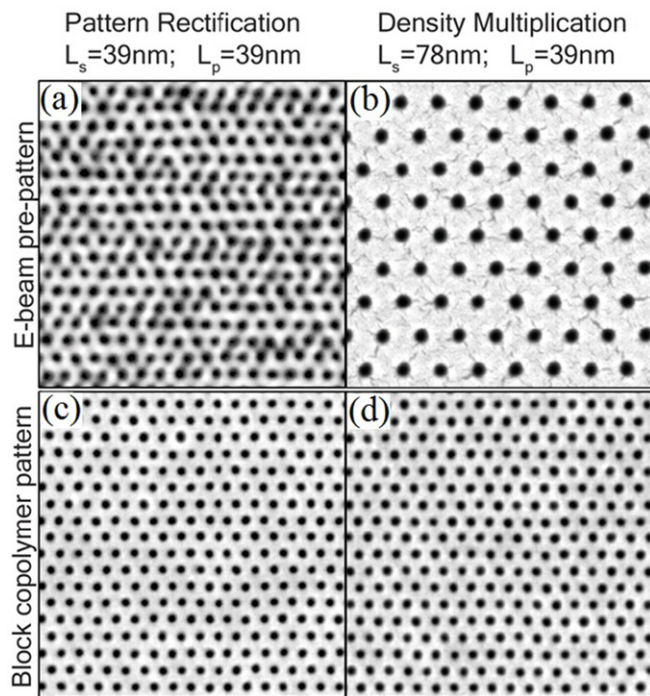
Figure 21. SEM images of developed e-beam resist ((a) and (b)) with $L_S = 39$ nm and 78 nm respectively. SEM images ((c) and (d)) of the block copolymer film on top of the prepattern defined by the corresponding e-beam pattern above. The lattice period on both of the BCP samples is 39 nm. Reprinted from [62] with permission from AAAS.

Figure 22. SEM images of PS-PMMA hexagonal patterns on three different molecular weight PS-OH brush layers ($M_n = 900$, 3700, 10 000 g mol^{-1}). The period of the prepattern and BCP are both 32 nm. Defects were determined from SEM images with 10 000 lattice points. Reprinted with permission from [94]. Copyright 2008 American Chemical Society.

10^{-3} limit required by BPM. Similar results demonstrating pattern rectification and density multiplication for PS-PMMA have also been demonstrated by Yang *et al* [39], including malformed and missing dots in the e-beam prepattern being repaired by the BCP process.

The effect of the molecular weight of the PS-OH brush layer was investigated by Tada *et al* [94] using a similar PS-PMMA system ($L_S = L_0 = 32$ nm). By using three different molecular weight PS-OH underlayers ($M_n = 900$, 3700, 10000 g mol^{-1}), variations in component structure were observed, with $M_n = 3700$ g mol^{-1} giving the fewest defects as observed by SEM analysis (figure 22). The authors compared these results with the contact angle of PS on the PS-OH underlayer. The contact angles for $M_n = 900$, 3700, 10000 g mol^{-1} were 24°, 6°, 0° respectively. The $M_n = 900$ g mol^{-1} PS-OH underlayer would have the poorest wetting of the overlying PS, and so this imperfection in coating may cause defects in the array structure. However, this does not correlate with the 0° contact angle having more defects than 6°, suggesting that arguments about wetting on the macroscopic scale may not be applicable on the nanometre scale. The authors suggest that more research into this trend is required.

Tada *et al* [94] also investigated whether density multiplication was dependent on the BCP film thickness. Lattice points were patterned with period $L_S = 64$ nm, where $L_S = 2L_0$. For a BCP film thickness of $t_f = L_0 = 32$ nm, density multiplication did not occur. PMMA cylinders on top of the patterned lattice points stood perpendicular, but PMMA cylinder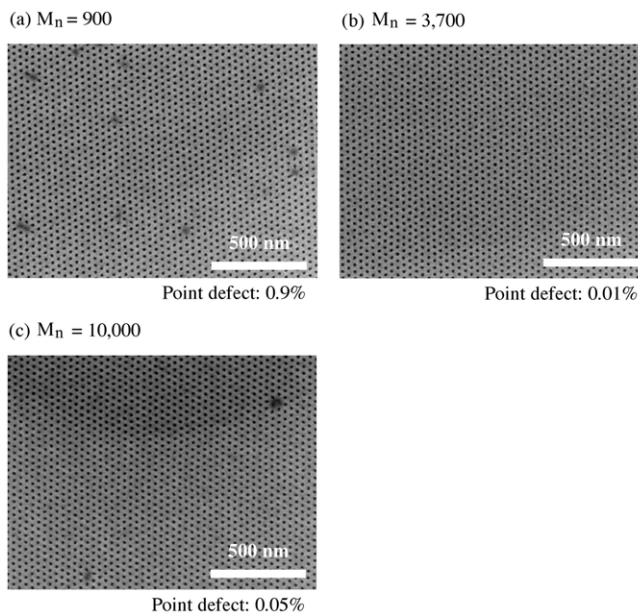s between the lattice points were orientated parallel to the surface. For a BCP film thickness of $t_f = 3/2L_0 = 48$ nm, density multiplication does occur, as all PMMA cylinders stood perpendicular. The authors' explanation is briefly summarized; For the thicker film if the cylinders were oriented parallel to the substrate surface, sterical filling of the film thickness would bring the PMMA chains in contact with the free surface, which is energetically unfavourable. Therefore the contact area between the two surfaces and the PMMA cylinders is minimized if the PMMA cylinders are perpendicular to the surface. For the thinner film the PMMA cylinders can instead orient parallel to the substrate with the PS contacting both surfaces.

The chemical prepatterning methods discussed so far rely on a positive tone resist with an underlying PS-OH brush layer. Sparse prepatterning with a negative resist (HSQ) has been demonstrated by Cheng *et al* [96]. Unlike with a positive resist, the areas of the HSQ resist which are exposed to the e-beam are cross-linked and become insoluble in the developing solution. They are preferentially wetted by PMMA, and were used to direct the self-assembly of lamellar PS-PMMA. In a separate study Wan and Yang [95] compared and contrasted a positive tone resist (ZEP-520) with that of a negative-tone resist (HSQ). Their e-beam exposure and development left very small posts (~5 nm height) of HSQ in a 'sea' of the underlying PS-OH brush (figure 23). They recorded a lower defect density when using HSQ versus ZEP-520 to form a hexagonal array of cylinder forming PS-PMMA and PS-PDMS ($L_0 = 24$ nm, $L_S = 24$ or 48 nm). 2D Fourier transform analysis showed many unusually small cylindrical pores and dislocated regions. These differences in defect densities could be attributed to the better e-beam resolution of HSQ over ZEP-520 at sub-25 nm periods, as no difference was observed in defect densities when
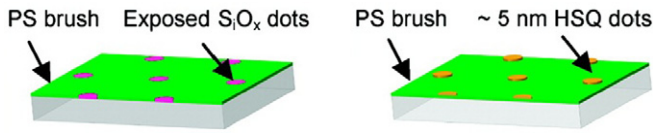
Figure 23. Two alternate methods of chemical templating. The positive resist method creates chemical contrast between a PS-OH brush and exposed SiO_x holes whereas the negative resist method generates chemical contrast between pillars ($\sim$5 nm height) of HSQ and a PS-OH brush. Adapted with permission from [95]. Copyright 2009 American Chemical Society.

using PS-PMMA with a greater lattice constant ($L_0 = 28$ nm) [30]. Furthermore, the O_2 dry etch may damage the uniformity of the prepatterned dots while transferring the pattern into the PS-OH brush layer. However, a significant downside is that HSQ resist requires a $\sim$10$\times$ higher e-beam exposure dose than ZEP520, resulting in a correspondingly longer e-beam write time.

7.1.2. Chemical vs topographical templating. Wan and Yang [95] also investigated the effect of the height of the HSQ posts on density multiplication. By using pillar heights of 5, 15 and 30 nm a direct comparison between chemical and topographical templating was able to be made. The 30 nm HSQ posts can be considered as a topographical template as they are comparable to the 40 nm film thickness (figure 24(*e*)), whereas the 15 nm pillars are considered to be intermediate between the two regimes.

Using a template consisting of a hexagonal array of 30 nm cylinders with $L_S = 87$ nm ($3L_0$), they achieved 9$\times$ density multiplication over the whole prepatterned area (figures 24(*a*) and (*c*)). 16$\times$ density multiplication was also attempted, although order was only obtained over a smaller 1 $\times$ 1 μm^2 area (figures 24(*b*) and (*d*)). Their attempt to achieve 9$\times$ density multiplication using chemical templating with the 5 nm HSQ posts gave undesirable results, with only short range order observed. Their results suggest that, with identical chemical properties and patterning features, topographical prepatterns can induce higher density multiplication than chemical prepatterns. This is because with topographical prepatterns the positions of the BCP components are physically fixed on every prepattern post, which decreases the possibility of defect formation.

7.2. Creating rectangular bits using chemical templating

Thus far, this section has focused on perpendicular-cylinder forming BCPs in hcp arrays. However, recently a new concept of BPM has been proposed that uses rectangular bits to store data [18, 69, 97].

Rectangular data bits have the advantage of a greater bit aspect ratio (BAR), where BAR is simply the ratio of the crosstrack width to the downtrack length of the bit. Such bit cells may enable the use of wider write-head poles, which can be desirable to achieve the high write fields and write field gradients needed to record sub-20 nm transitions on high coercivity media [20]. In addition, the magnetic read sensor width is approximately 70% of the track width, making the
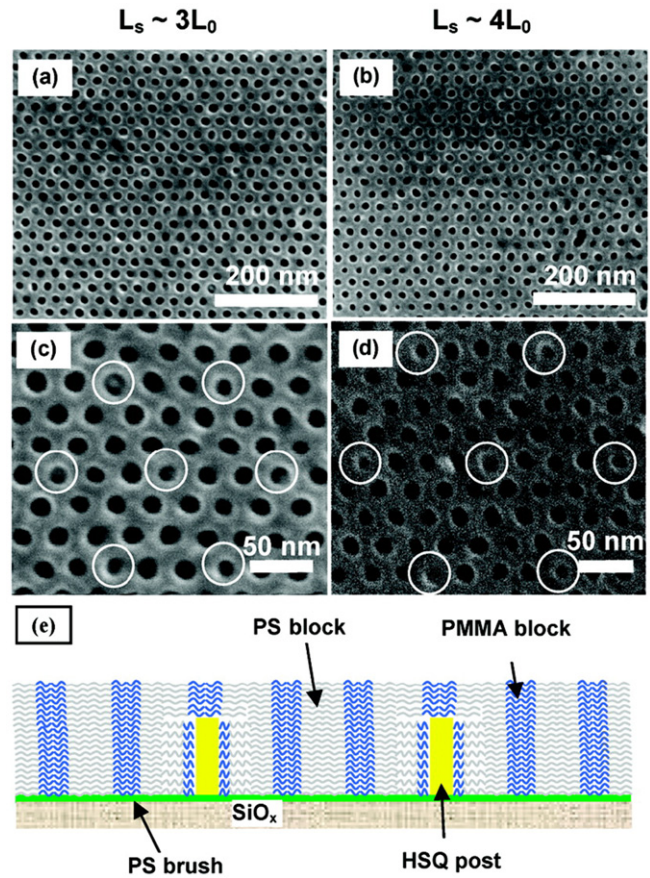

Figure 24. Top-down SEM images of PS-PMMA ($L_0 \sim 28.6$ nm) on top of 30 nm HSQ pillars with (*a*) $L_S = 87$ nm and (*b*) $L_S = 114$ nm. (*c*) and (*d*) are magnified images from (*a*) and (*b*), respectively. The circles indicate the BCP pores with HSQ posts in them. (*e*) Cross sectional diagram of PS-PMMA film on 30 nm thick HSQ posts with $L_S = 3L_0$. Reprinted with permission from [95]. Copyright 2009 American Chemical Society.

formation of the read sensor an important critical dimension [18]. The width of the read sensor is currently the smallest dimension in a disk drive and so scaling of this parameter should be minimized. There is also a mechanical budget for track misregistration (TMR) which is more relaxed if BAR $>$ 1. TMR describes the ability for the magnetic write/read-head to stay on track. In conventional magnetic recording the write-head is positioned within 10% of the track width, whereas the read-head is positioned within 15% of the track width. Incorrect positioning of the write-head can result in overwriting data on adjacent tracks, while poor read-head positioning can result in poor drive performance and multiple attempts to read data on successive revolutions of the disk. In BPM the problem is exacerbated by the need to compensate for the inevitable mechanical misalignment of the disk on the motor spindle.

Rectangular patterns are achievable by means of chemical patterning using a positive resist system similar to those described in section 7.1. However, because BCPs can only adopt a certain number of geometries, an additional e-beam step is required. Although time consuming, the additional e-beam step will only need to be carried out once if a master template is being created [69]. The process demonstrated by
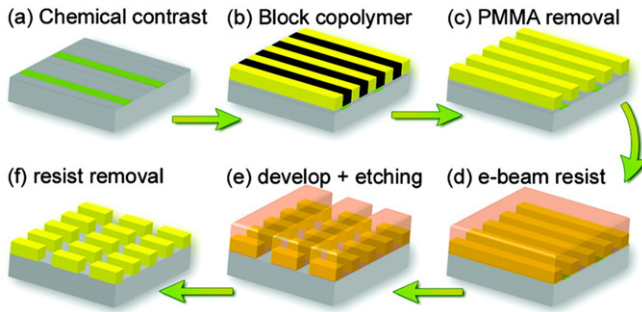
Figure 25. Fabrication of rectangular patterns from lamellar phase BCP stripes. (*a*) Chemical contrast created on substrate with sparse lines. (*b*) BCP aligns with substrate (density multiplication). (*c*) PMMA is removed from the polymer film. (*d*) E-beam resist is deposited over PS stripes and an orthogonal stripe pattern is written by e-beam. (*e*) E-beam resist is developed and exposed areas are removed. (*f*) Remaining 'unexposed' resist is removed to leave an array of rectangular features. Reprinted with permission from [97]. Copyright 2011 American Chemical Society.

Ruiz *et al* [97] is shown in figure 25. EBL is used to write a sparse stripe pattern into a layer of PS-OH (figure 25(*a*)). Lamellar phase PS-PMMA is applied and thermally annealed to form the lamellar pattern shown in figure 25(*b*). The PMMA component is then selectively removed with oxygen plasma to leave stripes of PS (figure 25(*c*)). Following this a new film of e-beam resist is deposited (figure 25(*d*)) and an orthogonal stripe pattern is written by EBL. Oxygen plasma is used to remove the exposed stripes (figure 25(*e*)), so that when the remaining resist is removed (figure 25(*f*)), an array of PS rectangles is left.

The PS-PMMA used in these experiments had a period of $L_0 = 27$ nm. Chemical prepatterns were written with $L_S = 2L_0$ and $L_S = 3L_0$, demonstrating 2× and 3× density multiplication in one dimension. The orthogonal stripe pattern was written with a period of 54 nm ($2L_0$), defining a rectangular lattice with an aspect ratio of 2. However, any period can be used, allowing rectangles to be formed with any BAR.

Figure 26 shows a top-down SEM micrograph of the rectangular PS patterns at the end of the process as well as a side view from a 10° tilt angle. Image analysis was performed on a $2.5 \times 2.5 \, \mu m^2$ array of rectangles. The standard deviation of placement error in both the *x* and *y* directions was below the 5% required for BPM. Size distribution analysis gave the average length of the short side (downtrack) of the rectangle which is defined only by the BCP as 16.3 nm, with a standard deviation of 0.49 nm (3.0%). The long side (crosstrack) whose resolution is determined by EBL alone had an average length of 41.3 nm with a standard deviation of 1.3 nm (or 3.1%). As a percentage, e-beam deviation values tend to increase with smaller dimensions, highlighting the advantage of using BCPs for the critical dimension.

7.2.1. Skew. In current HDD designs, the read/write head is mounted on a slider. As the slider moves across the disk it follows an arc rather than a straight line. To match this non-radial movement, the BCP lattice structure requires a skew angle between approximately ±15° [39], with tracks near
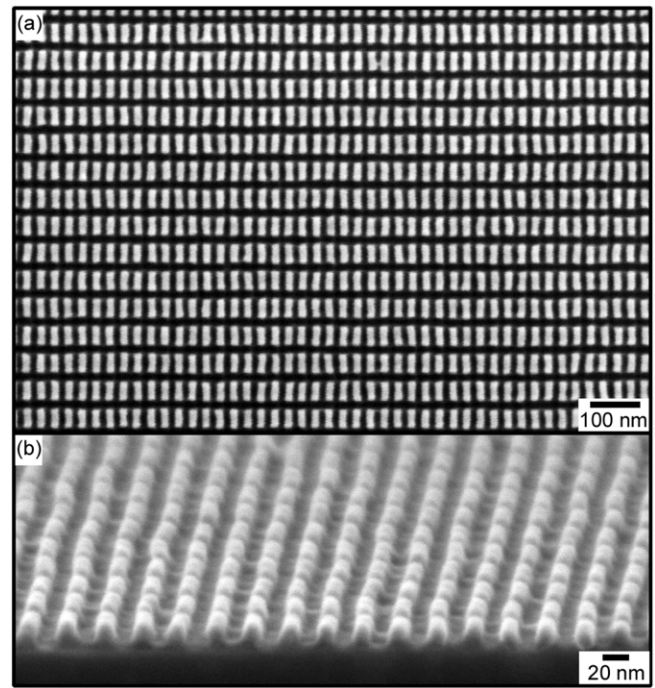

Figure 26. SEM micrographs of PS rectangular patterns. (*a*) Top-down view. (*b*) View from a 10° tilt angle. Reprinted with permission from [97]. Copyright 2011 American Chemical Society.

the inner region of the disk having a skew in one direction, passing through zero skew somewhere in between. Previous studies using hcp BCP patterns have attempted this by using a skewed prepattern [39], but order has only been maintained up to 8° [98, 99] due to the stretching and compression of the polymer chains. This is another advantage of using rectangular bits as an arbitrary skew angle can in principle be obtained by writing stripes in the second e-beam exposure (figure 25(*d*)) at a non-90° angle. This has been demonstrated by Lille *et al* [18] with 1.3 BAR bits at a skew angle of 9°.

7.2.2. Double imprint lithography. Further work by Wan *et al* [69] using chemoepitaxy and NIL has enabled both sides of the rectangular bits (crosstrack and downtrack) to be fabricated using DSA of BCPs. In this work the rectangular bits are fabricated on circular tracks using a double imprint process (figure 27). Two submaster templates with circumferential and radial lines are created separately before being combined through a double imprint step to create a master template. The fabrication process utilizes a rotary stage e-beam system which is able to write both the circumferential and radial line patterns into a ZEP-520 resist (on top of a PS-OH or XPS brush layer).

The circumferential line submaster was formed by e-beam exposure at 54 nm period (figure 28(*a*)), which was double the period of the PS-PMMA BCP ($L_0 = 27$ nm). Following standard lithographic steps, the BCP was spin-coated and annealed on the substrate. The BCP lamellae could follow the curvature of the circumferential lines because this negligible curvature at large radius is well below the curving tolerance in block copolymer films. The PS blocks were then transferred into the Si substrate using a Cr hard mask and RIE process, as
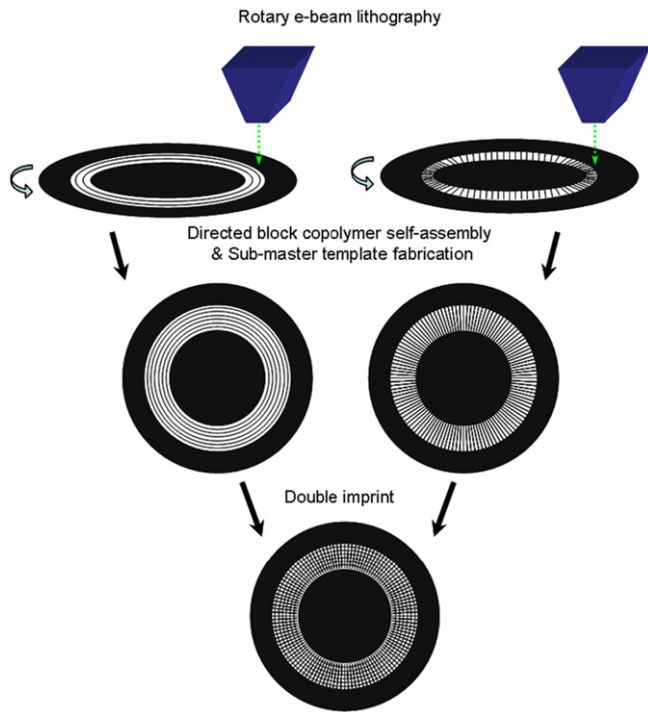
Figure 27. Rotary EBL and DSA of BCPs used to create two submaster templates which in turn are used to make a master template via a double-imprint process. Reprinted with permission from [69]. Copyright 2012 Society of Photo Optical Instrumentation Engineers.

can be seen in figure 28(*d*). Although circular in reality, the lines appear straight in figure 28 due to the negligible curvature over the area of this SEM image. The Moiré interference pattern in figure 28(*e*) demonstrates the long range order of the circumferential lines.

For the radial line submaster, the patterns were separated into many zones along the radial direction with the angular period kept constant within each zone (figure 29), but decreasing the angular period for zones increasingly further from the centre, so that the bit period is roughly constant in all zones. This technique prevented the radial lines from becoming too sparse at the outer diameter. The period of the radial lines (L_S) was chosen to be equal to the natural period (L_0) of the BCP in the middle of the zoned regions and varying ±1% within a zone.

Two radial line submasters were produced using similar lithographic methods, one with a 41 nm period, and the other with a 27 nm period. To demonstrate the double imprint process, the 27 nm circumferential line submaster was used together with the 41 nm radial line submaster to obtain a final master template with rectangular bits arranged in pseudo-rectangular arrays, with an areal density of 0.58 Tb in^{-2}. This was carried out by sequential imprints and RIE on a Cr-coated quartz substrate to produce rectangular Cr islands. The substrate was then etched with a fluorine-based RIE to form rectangular protrusions with a height of 20 nm.

A primary concern with this double imprint process is that the submaster templates require meticulous alignment with the master template. A mismatch error in the double imprinting
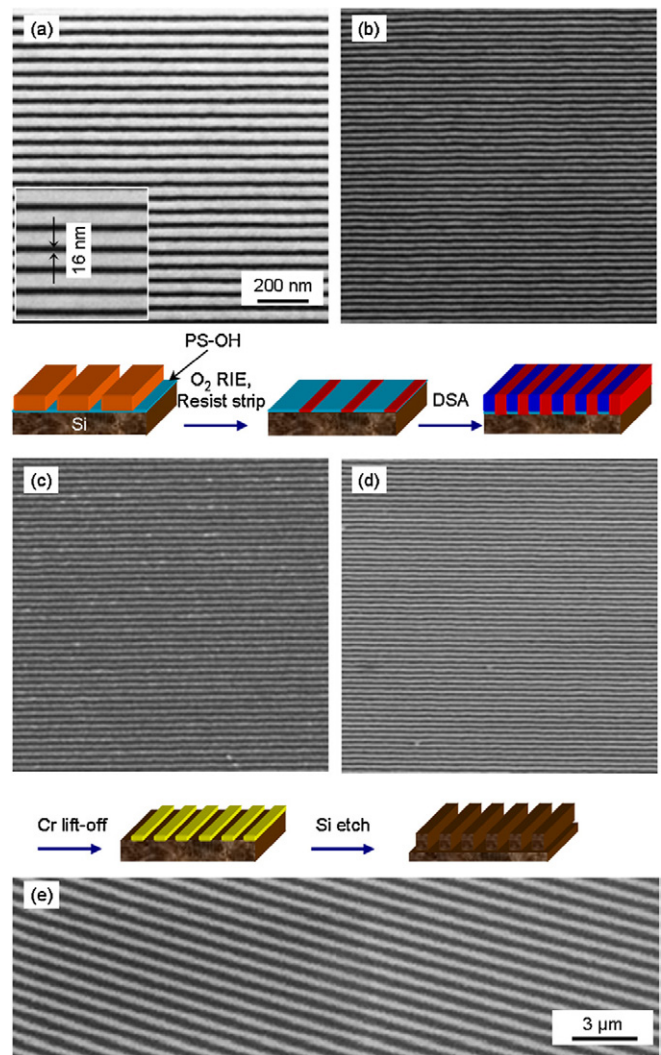
Figure 28. Fabrication of nanoimprint template with circumferential lines from BCP lithography. (*a*) ZEP resist pattern of 54 nm period ($L_S = 54$ nm) circumferential lines defined by rotary EBL. (*b*) Chemical contrast pattern generated by O$_2$ RIE and resist stripping. (*c*) Lift-off process to generate Cr stripes. (*d*) Si wafer etched using Cr as mask. (*e*) Moiré interference pattern of the template. Reprinted with permission from [69]. Copyright 2012 Society of Photo Optical Instrumentation Engineers.

Figure 29. Zoning of radial line patterns. Adapted with permission from [69]. Copyright 2012 Society of Photo Optical Instrumentation Engineers.

steps could render certain data areas unusable. The authors' target of ~1 μm alignment can potentially be achieved by conventional optical or interferometeric techniques handled by the nanoimprint tool.

J. Phys. D: Appl. Phys. **46** (2013) 503001

Topical Review

8. Creating servo patterns with BCPs

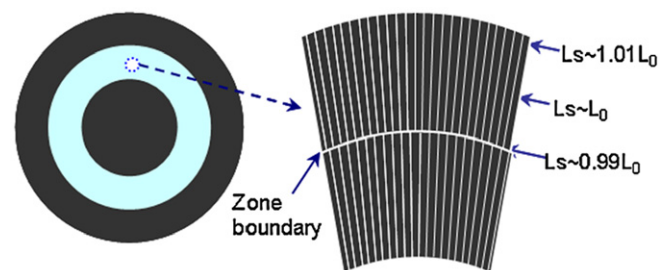Along with tracks or bits, additional features termed servo patterns are included on hard disks to enable the head to read and write data at precise locations. The design of servo patterns plays a key role in the performance of the disk drive, and these patterns are typically proprietary to each drive manufacturer. Servo patterns contain features with dimensions that are typically $2\times$ to $10\times$ larger than the data features and include arrays of lines and dots. Servo patterns are placed at regular angular intervals around the disk, with the effect of dividing the disk surface into a large number of wedge-shaped sectors. A typical disk might be divided into 100–400 sectors, with servo patterns occupying 5–20% of the active surface of the disk [100].

In current hard disk technology the data are written on to a featureless continuous medium. As there are no preset track locations, the servo marks are written onto the disk with a recording head. The servo writing process consists of flying the head over the entire disk surface and recording the servo marks. It is a serial process that is both slow and expensive [5], so if the throughput of this process could be improved or negated altogether, there is a potential for significant cost savings.

With BPM, the track locations are predefined and thus the servo marks will also need to be patterned. A potential advantage of this is that it removes the slow servo writing step from the manufacturing process. However, the servo marks cannot be separately written by EBL as the alignment is too poor [97]. Even state-of-the-art alignment capability would not meet the registration requirements of a hard drive's tracking tolerances (1 nm) [101]. This servo mark requirement means that methods capable of producing only purely periodic, isotropic, bit patterns which fill the entire disk are not sufficient [5]. This is a significant challenge when using BCP self-assembly to produce BPM. Many conventional servo pattern features do not correspond to the types of periodic features most easily formed by the free energy minimization process that orders BCPs [102].

Another option would be to start with a common e-beam pattern for both data and servo, and subsequently process the two types of area separately. This approach would provide self-registration of servo and data, and like the option above, allows for arbitrary servo patterns combined with data patterns created by BCP self-assembly. A challenge with this approach is development of an integrated process that does not compromise the quality of the delicate BCP lithography process for the data islands [101].

Current efforts are focused on two different techniques. One is to use chemoepitaxy to coerce the BCPs to assemble into servo patterns. The other is to use graphoepitaxy, where the servo patterns are directly written as trenches which are filled with BCP.

8.1. Servo formation by chemoepitaxy

Ruiz *et al* [97] have previously shown how rectangular bits can be formed from lamellar BCP patterns. In a subsequent paper by the same group, Liu *et al* [103] have shown how
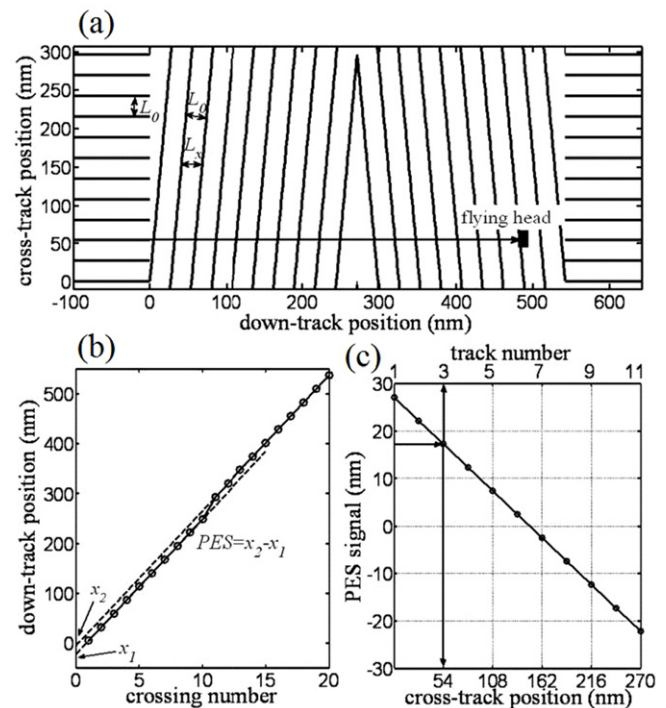

Figure 30. (*a*) Chevron structure design to extract the position error signal (PES) for magnetic data storage. There are 11 tracks ($n = 1, 2, 3, ..., 11$) with cross-track positions of 0, 27, 54, ..., 270 nm, respectively. (*b*) One exemplary collection of the signals while the head is flying across the chevrons following the arrow in (*a*). The abscissa denote the crossing number at which the head crosses the chevrons. The ordinate is the down-track position when the head crosses the chevrons. The dashed lines are extrapolations of the fitting lines to the data, and the intercepts are x_1 and x_2. The PES $= x_2 - x_1$. (*c*) The PES as a function of the position of the head across the track direction. The solid circles denote the points where the head is flying on the track. The arrows in (*c*) illustrate the identification of a cross-track position of 54 nm, or a track number of 3, when the read-head flies along the arrow highlighted in (*a*). Reprinted with permission from [103]. Copyright 2011, American Vacuum Society.

chemoepitaxy can bend lamellar patterns into a chevron shape suitable for a servo. In this preliminary study the work was not taken through to transferring to a magnetic layer, and the data tracks on each side of the servo feature were left as lamellae rather than being divided into rectangles.

A chevron design is shown in figure 30(*a*) where the chevron servo feature is placed at the start of a data sector. As the head flies along a data track, it will detect (once the lamellae are divided into rectangles) a certain frequency, f, proportional to the bit spacing. This frequency will change when it enters the servo area. On the left of the apex of the chevrons, the frequency will be v/L_x, where v is the head velocity along the down-track direction, and L_x is the apparent spacing along the down-track direction. On the right of the apex of the chevrons the frequency will be the same, but there will have been a phase-shift due to crossing the midpoint. From figure 30(*a*) it can be seen that if the head were on track 2 (cross-track position 27 nm), there would be a length of time where no magnetic transitions are present corresponding to a large positive phase-shift. If it were on track 10, there would be
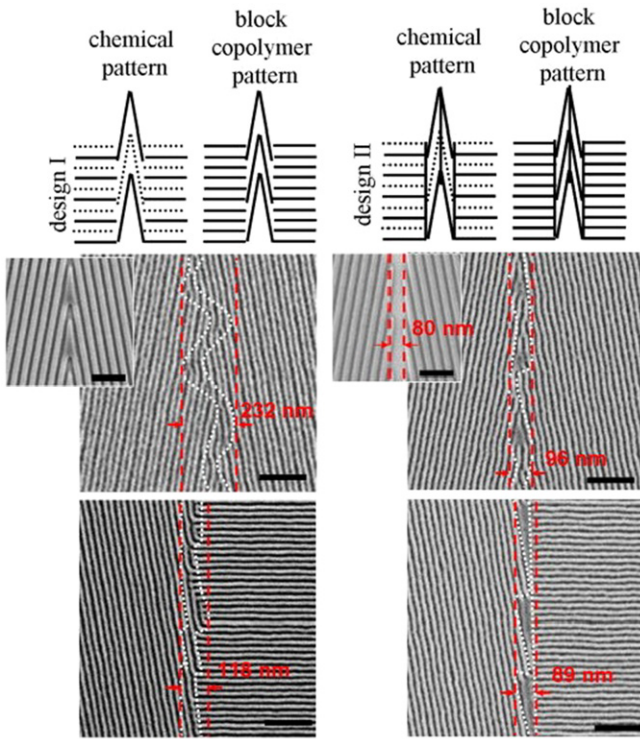
J. Phys. D: Appl. Phys. **46** (2013) 503001

Topical Review

Figure 31. Chevron design schematics and resulting lamellar patterns. For design I and II schematics (shown at the top), the solid lines represent the e-beam prepatterns at a period of $2L_0 = 54$ nm, whilst the dotted lines represent lamellae interpolation giving $2\times$ density multiplication. In design II extra vertical e-beam prepatterns were added. SEM images of the resulting lamellae ordering is shown below. The red dashed lines indicate the boundaries between defective and non-defective areas. The widths of the design II defective areas are smaller as a result of the additional vertical prepatterns. Reprinted with permission from [103]. Copyright 2011, American Vacuum Society.

a large negative phase-shift. Figure 30(*b*) shows the phase shift being used to calculate the position error signal (PES) value. Figure 30(*c*) shows a lookup chart of values—the expected PES value can be identified for that track. When the head crosses the chevrons the HDD controller can compare the detected PES with the expected value for that track, and use that comparison to correct the head position.

Figure 31 shows two different e-beam designs (20° chevrons) with SEM images of the resulting BCP patterns (lamellae BCP periodicity L_0 of 27 nm). The EBL designs utilize $2\times$ density multiplication as can be seen by the dotted lines (figure 31—design I and design II) showing the 'missing' EBL lines where BCP will self-assemble. Bending the BCP lamellae at sharp angles involves a high free energy penalty, and this results in defects at the chevron apexes as well as the junction between the horizontal tracks and chevrons. The width of these defective and therefore unusable areas has been highlighted by the red dashed lines.

In design II, additional vertical lines were added at the apex of the chevrons, as well as at the transition vertices between the horizontal lines and the chevron lines, as can be seen by comparing the design II schematic with the design I schematic. The defects were different from those in design I, and the widths of the defective areas are smaller. Parallel lamellae
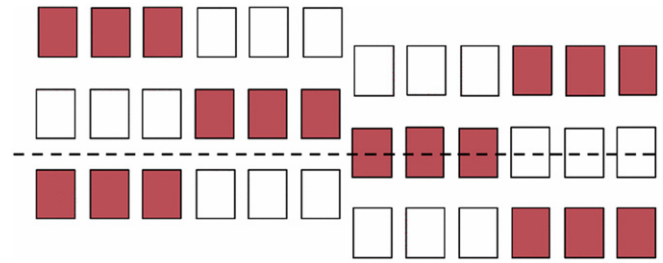

Figure 32. Diagram of an offset field pattern. Track centre represented with dotted line. This is shown for a scheme which has islands of alternating magnetic polarity as represented with alternating coloured islands. Reprinted with permission from [101]. Copyright 2012 IEEE.

formed in areas subject to a relatively high e-beam dose. As a result, the defective structures remained localized and barely propagated to the periodic line pattern areas. The chevrons can still provide PES information despite these defects, but it would be necessary to determine the widths of the unusable areas at the chevron apexes as well as at the chevron edges, where data cannot be stored.

In a subsequent paper, Lille *et al* [101] propose that although the chevron design could be used to provide PES data, other servo features which are not as amenable to BCP assembly (such as track number, sector number and various synchronization features) would need to be written magnetically during a servo writing operation on islands which are identical to data islands.

The authors also examine an alternative PES servo design that could be formed by BCPs, shown in figure 32. This pattern consists of an offset field identical to data islands in every respect, except that the track boundaries are shifted by a fraction of a track relative to the data tracks. Like the chevron pattern, this only requires a slight change during the e-beam exposure to set up track positions [101]. For islands with dc magnetization, a simulation predicts that the chevron pattern would offer ~20% greater readback signal than the offset field pattern. For islands of alternating polarity magnetization the simulation predicts that the readback signal of the chevron and offset field patterns would be similar. Alternating polarity magnetization provides a ~27% signal improvement compared to the dc chevron pattern, presumably due to the greater contrast between areas of opposite magnetization. The extra signal provided by alternating magnetization would need to be balanced against the extra time required for servo writing this during production.

Further work is required in order to fabricate an offset field pattern with chemoepitaxy and see whether it forms with fewer defects than a chevron pattern, which might be expected due to reduced strain in the system. However, as it is an amplitude pattern it is still likely to be less well suited to BPM than the phase based chevron pattern (explored further in the next section).

8.2. Servo formation by graphoepitaxy

To bypass the problems of coercing BCPs to form servo patterns, graphoepitaxy can be used instead, where BCPs are
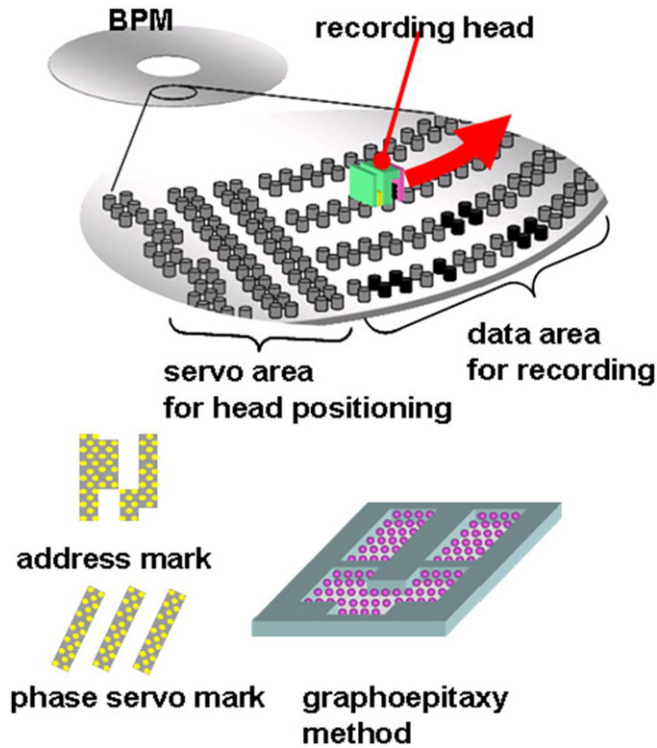
Figure 33. Schematic images of servo patterns formed by graphoepitaxy. Reprinted with permission from [104]. Copyright 2012, American Vacuum Society.

Figure 34. Calculated read-back signal from a model graphoepitaxial servo pattern. The magnetic recording medium is divided by a mesh of size 10 nm × 10 nm × 10 nm. The widths of the ridge and groove portion are both 100 nm. The angle of ridge-and-groove guide to the direction of the data track is 45°. Reprinted with permission from [107]. Copyright 2011 IEEE.

Figure 35. Calculated PES and linearity error from a model servo pattern. Reprinted with permission from [107]. Copyright 2011 IEEE.

deposited into grooves written by EBL in the shape of servo patterns. Figure 33 shows schematics of servo patterns formed in this way.

This section will begin by considering simulations that have been undertaken for graphoepitaxy created servos, followed by fabrication experiments.

8.2.1. Modelling servo patterns. Previous papers have analysed the performance of PES servo patterns for BPM [105, 106], and consider a phase based servo to be more suitable than an amplitude based servo. Dot size dispersion of BPM results in amplitude fluctuation noise and degrades the amplitude servo signal, whereas a phase pattern servo has tolerance against the amplitude noise.

This was demonstrated by Kamata *et al* [107] when they estimated the suitability of a phase pattern fabricated by graphoepitaxy. A simulation was run where there is a low density of magnetic bits within the lines of dots making up the servo pattern. This model represents a BPM with completely disordered 10 nm dots whose average period is 20 nm. The area dot density is 25% and random dot alignment was assumed to be worst case. Figure 34 shows an image of this model phase pattern and the simulated output signal when flying a head.

At the left-hand side of the inset to figure 34 the sensitivity distribution function of the read-head can be seen. In this simulation the read-head has a width of 70 nm, gap of 35 nm and flying height of 4 nm. Since the read-head width is larger than the dot size, the signal is averaged over several dots. The random nature of the dot density in the stripes leads to a
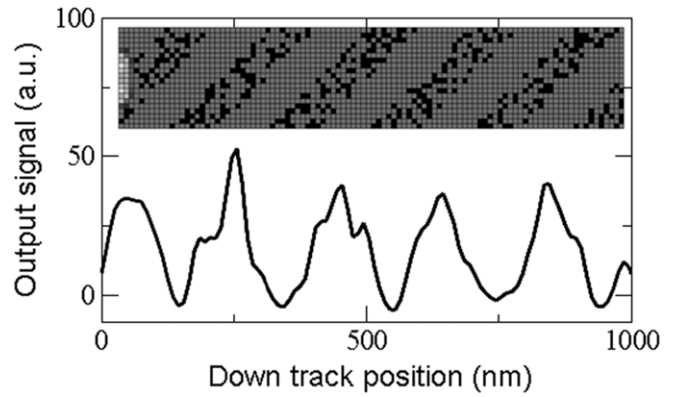
distorted output signal as shown in figure 34. The amplitudes of the peaks fluctuate by up to 50% which would lead to a non-linear PES in an amplitude based servo pattern. However, a phase based servo pattern works based on the locations of the peaks rather than their amplitudes. The calculated PES based on the peak locations shown in figure 35 has good linearity, which is an important property for high-precision head control.

Another simulation was run with more realistic values of 5.5% dot size distribution and 6.5% dot period distribution. Figure 36 shows calculated PES linearity error as a function of a read-head width. For comparison, the PES linearity error of a model without distribution of dot size and position (ideal model) was calculated. For the case of a read width of 60 nm, the PES linearity error 1σ calculated from the model with realistic parameters is 0.3 nm. This number is smaller than the deviation of the dot period (2.4 nm). In an actual BPM system the read-head width must be less than the dot period in order to avoid noise from adjacent tracks, so 15 nm read-head width is more realistic. This causes the PES linearity error to increase

Figure 36. Calculated 1σ PES linearity error from the realistic model (with deviations) and the ideal model (without deviations). Reprinted with permission from [107]. Copyright 2011 IEEE.
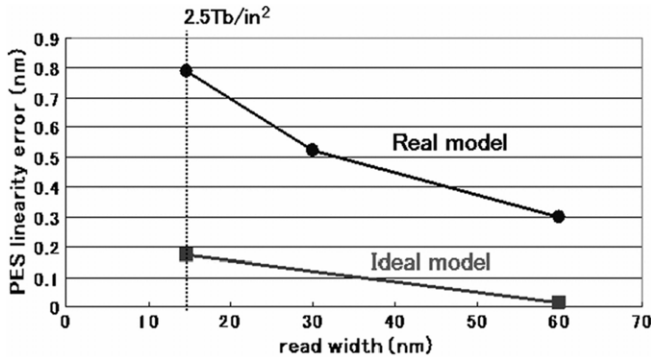
to 0.8 nm, so commensurate reductions in dot size and period variation are required to achieve the same PES linearity error. The authors also speculate that this value could be reduced to 0.1 nm with the use of a low-pass filter.

The above models do not take into account the effect of LER of the grooves which causes deviation in the positions of the dots. This additional deviation will also cause PES linearity error [107].

Although a phase based pattern is less susceptible to amplitude fluctuation noise than an amplitude based pattern, both patterns are susceptible to dot position fluctuation that results in timing jitter noise. Simulations conducted by Han and Callafon [108] show an alternative phase based pattern termed the 'differential frequency pattern' to be least susceptible to these noise sources, although to our knowledge this has not yet been fabricated using BCPs.

8.2.2. Fabrication of servo marks. Circular BPM with servo marks have been fabricated using graphoepitaxy at densities of 0.8 and 2.5 Tb in^{-2} by Yamamoto *et al* [109]. Figure 37(*a*) shows a schematic of the design. Data tracks are at both sides of a servo design consisting of an address mark (for random access of the recording head), preamble marks (information on the clock frequency for the recording and reading data), and a phase pattern (for PES). This design was fabricated by creating the groove guides with EBL, filling them with PS-PDMS and annealing. 0.8 Tb in^{-2} density was fabricated by using a BCP with 33 nm period. AFM images of this are shown in figure 37(*b*) (boundary region between the data track area and the phase servo area) and figure 37(*c*) (boundary region between phase and address servo patterns).

A 2.5 Tb in^{-2} density medium was formed using PS-PDMS of period 17 nm, as shown in figure 38. In figure 38(*b*) it can be seen that the dots are still ordered in spite of the groove width variation. However, it can also be seen that the edges of the grooves have LER. This design was not tested on a spinstand so it's not certain what effect this 'blurring' of the servo patterns has on their performance. The 1σ variations in dot period and diameter were 14.6% and 15.7% meaning that further optimization of that fabrication method is needed in order to reduce the variations to a level suitable for BPM. However, it has shown that arbitrary servo patterns
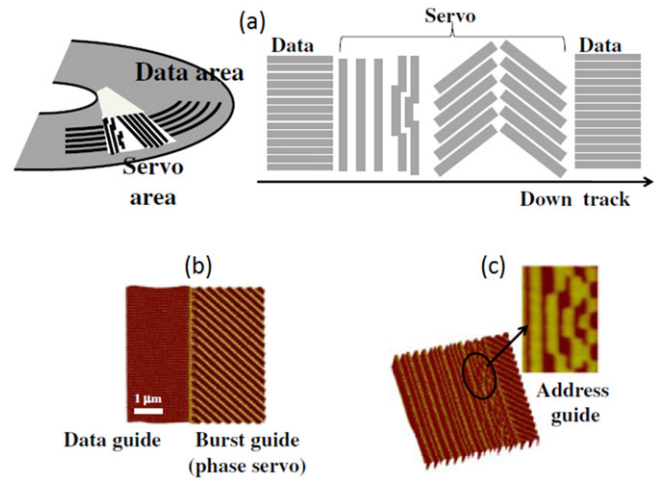
Figure 37. (*a*) Schematic of track and servo grooves. (*b*) and (*c*) show AFM images of the groove guides on the 0.8 Tb in^{-2} design. Reprinted with permission from [109]. Copyright 2012 The Japan Society of Applied Physics.
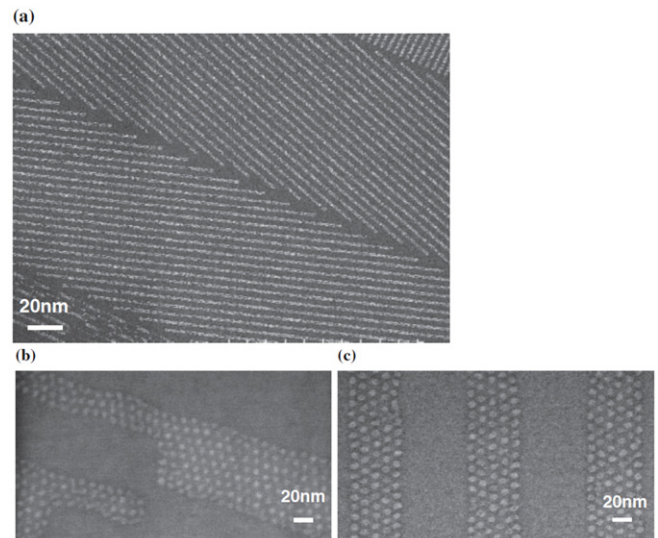
Figure 38. Plan-view SEM images of the PDMS dot array (*a*) around the phase servo mark area, (*b*) on address mark area, and (*c*) on data track area for 2.5 Tb in^{-2} DSA-BPM. Reprinted with permission from [109]. Copyright 2012 The Japan Society of Applied Physics.

can be formed for high density BPM using graphoepitaxy. A subsequent paper reported fabrication of servo features using graphoepitaxy at density 5 Tb in^{-2}, although similarly no spinstand results were reported [104]. Further work is required to test these designs and evaluate the tolerance of all the servo features to LER, line width roughness, as well as dot size and placement deviations.

9. Mass production of BPM using NIL

As introduced in section 2.1.1, NIL can use a master template produced by BCP DSA to imprint many substrates. This section will review progress towards achieving the quality and throughput requirements for mass production of BPM HDDs.
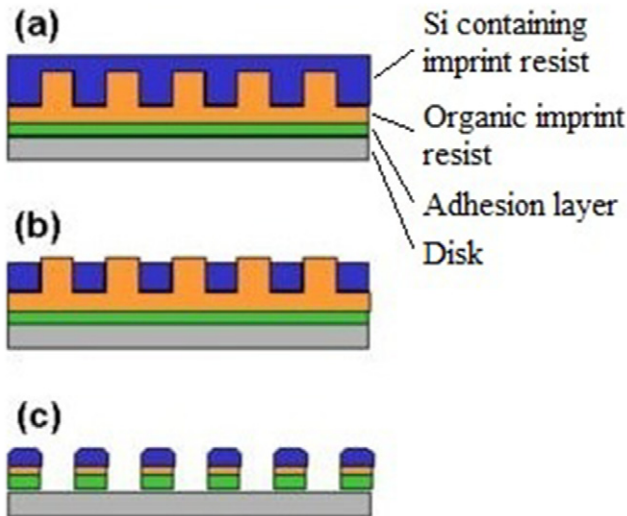
Figure 39. An example reverse tone process. The organic imprint resist (Monomat) has already been imprinted by a pillar-tone template. (*a*) A silicon containing imprint resist is dispensed on the Monomat, and a thin blank fused silica template is used to planarize the silicon containing resist and fill the holes. (*b*) An etch back process using CHF_3/O_2 RIE is used to etch off enough silicon containing resist to expose the Monomat resist pillars below. (*c*) An O_2 RIE process is next used to remove the exposed Monomat resist leaving behind silicon containing pillar-tone features. Adapted with permission from [110]. Copyright 2008, American Vacuum Society.

NIL can use either a pillar tone template to produce holes in the resist, or a hole tone template to produce pillars in the resist. Resist pillars can be converted into BPM using one of the methods described in section 5.3. Therefore a hole tone template is preferred for simplicity, however it is much more difficult to fabricate [110].

One solution is to fabricate the master template as a pillar tone template. This can imprint substrates covered with resist to produce daughter templates which would have a hole tone. These daughter templates could then imprint resist covered 'granddaughter' substrates to produce resist pillars which would be transferred into BPM. The production of many daughter templates has advantages in throughput and cost as explained in section 9.2.

Another solution is to avoid hole tone templates with the use of reverse tone processing [110]. A pillar tone master is used to imprint resist. The resist holes are then converted into pillars by a reverse tone process such as that shown in figure 39, which entails an additional imprint step (with a blank template), and two etching steps. A variation of this technique has been used by Albrecht *et al* [52] who substituted the initial blank template imprint of Si containing imprint resist with vacuum deposition and etchback of a metal fill material. They suggest this will be more easily scalable to mass production. The pillar tone template that results from reverse tone processing can be used as a daughter template, and the process repeated to produce many granddaughter substrates with resist pillars that can be transferred into an underlying magnetic layer. Although reverse tone processing adds complexity, the elimination of hole tone templates has several advantages (highlighted in the following sub-sections), leading

reverse tone processing to become the standard technique used by industry.

As described in section 2, BPM placement and size distributions must be no greater than 5% (1σ). In addition there are limits placed on defectivity (e.g. missing or deformed bits). HDD signal processing changes in the past decade mean that raw error rates in the 10^{-2} range can now be tolerated [26] which is very different from the 10^{-6} range required 10–15 years ago. This has relaxed BPM defectivity requirements with a 10^{-3} defect level in the media itself now being a target, thus being only a 10% contributor to an overall error rate of 10^{-2}. Bad sectors with a defect rate higher than 10^{-3} can be mapped out.

Most variation and defectivity occurs during the template fabrication steps, particularly the first step of defining dot sizes and positions with EBL (BCP self-assembly was shown in the previous sections to reduce this variation). In order to keep the size and position variation at an acceptable level, it is critical that the imprint step does not introduce a significant amount of additional variation or defectivity. Factors that can cause a lack of fidelity in NIL will be examined in the next section.

9.1. Bit variation and defectivity

In the NIL process the template first needs to be overlayed onto the resist. Basic alignment on the order of tens of micrometres is required to ensure the pattern is properly centred on the disk [100], as the disk will not be centred to better than approximately $10\,\mu m$ on the drive spindle [5]. BPM is formed in a single lithographic processing step, so the nanometre precision necessary when aligning with previous layers is not required.

When the template is pressed onto the resist covering the substrate, there will still be a thin layer of resist left beneath the template features, termed the residual layer. A base layer etch (descum) is subsequently carried out to remove the residual layer. Variation in residual layer thickness (RLT) means that sufficient descum must be carried out to remove both the thicker and thinner regions, causing the desired resist features to be eroded by varying amounts. This leads to critical dimension (island diameter) variation [111]. RLT variation is mitigated by controlling how the resist is applied onto the substrate. Rather than spin-coating a layer of resist, jet and flash imprint lithography (JFIL) (Also called step and flash imprint lithography (SFIL)) uses an inkjet head to deposit picolitre volume droplets (typically $\sim$5 pL but as low as 1.5 pL [112]) across the surface, with a density that matches the local pattern density of the template. Figure 40 shows uniform residual layers resulting from this technique with a thickness of 15 nm. Measurements of the RLT when using JFIL to imprint from a 1 Tb in^{-2} BPM template gave a mean value of approximately 8 nm [113]. The effects of RLT variation are further mitigated by using reverse tone processing, as a filler material in the resist holes is used as the etch mask, rather than the resist pillars themselves.

Non-fill defectivity occurs when the resist does not completely fill the template features. This is more likely to happen if the resist is too viscous, or has been spread
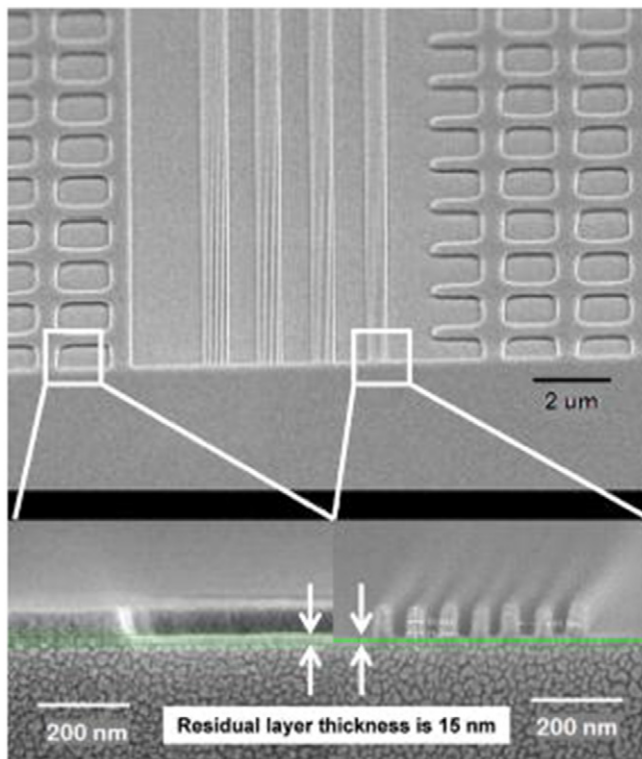
Figure 40. Resist dispensing using inkjet drop-on-demand technology rather than spin-coating enables uniform residual layers to be obtained across the entire substrate, independent of pattern density and feature size variations. Reprinted with permission from [100]. Copyright 2009, American Vacuum Society.

Figure 41. (*a*) Imprinted pattern showing resist collapse. (*b*) Patterns free of resist collapse. Reprinted with permission from [115]. Copyright 2012 Society of Photo Optical Instrumentation Engineers.

imperfectly. This can be mitigated by locally dispensing small droplets as with JFIL, so that all areas of the substrate have the required amount of resist to fill the template features. An additional aid is to bend the template as it's pressed onto the resist [114]. This causes liquid contact to start at the centre and move outwards, which helps to expel air that would otherwise occupy volume beneath the template. In addition, part of the pattern may be torn if the cured resist adheres to the template, so surface treatments of the template are critical in ensuring high reproduction fidelity [4].

Resist collapse (where the tops of features coalesce and stick together) becomes an issue as bit density increases. In the case of BPM at sub-20 nm feature sizes, resist collapse is manifested as the formation of doublets or triplets where two or three resist pillars collapse together as shown in figure 41(*a*). This can be mitigated by using a resist of higher tensile modulus (so the resist features are stiffer and more resistant to bending), and by reducing the height of the template features. Choice of resist and usage of a height/diameter aspect ratio of 2 : 1 enabled resist collapse to be eliminated in sub 15 nm bits, as shown in figure 41(*b*) [115]. This must be balanced against the consideration that lower height of the resist features will leave less margin for error in the subsequent etching process. Alternatively if reverse tone processing is in use, the resist can be imprinted with a pillar tone template to leave a continuous network with holes in it. This is less likely to coalesce than isolated pillars.

Particle defects are a concern—the large relative size of many particles in comparison to nanoscale BPM means they can cause wide area damage. If the particle stays stuck to the template, it will repeatedly damage resist patterns, and hard particles have been shown to cause permanent damage to the quartz template [116]. Ensuring a particle free process is a challenge, though one where the process steps developed by the semiconductor industry will be useful.

Cleaning of stamps becomes necessary if resist residues adhere and/or become lodged within the features of the stamp (called template fouling) [117]. Therefore it is necessary to develop cleaning processes for both particle and organic residue removal. Traditional template cleaning utilizes a sulfuric acid and hydrogen peroxide mixture, called SPM, which removes crosslinked resist. The SPM process is known to be very effective in removing organic residues. However, concerns over residual ion control, waste chemical management and thermal cycling, limits the use of SPM for NIL template cleaning [118]. UV/ozone/SP1 acid-free

J. Phys. D: Appl. Phys. **46** (2013) 503001

Topical Review

cleaning processes have also been shown to be effective [34]. In addition, various physical force wet cleaning methods are employed to remove nano-sized particles [118].

9.1.1. Analysis of variation. Analysis of the contribution of variation at each stage (from master template fabrication to imprinting) has been performed by Yang *et al* [119]. Their results based on limited samples show that at 250 Gdot in^{-2}, the 1σ size variation is 3.1% in ZEP520 resist when patterning dots using EBL. This increases to 3.3% after pattern transfer to the quartz template and 3.5% after disk imprinting, showing that most of the variation occurs when producing the master template rather than imprinting. A quite similar trend is also found in the higher density samples but with an additional increase of 1–2% at 500 Gdot in^{-2} and 2–3% at 720 Gdot in^{-2}. For the 1.1 Tb in^{-2} sample, a significant increase in the 1σ value due to the higher defect density is seen. The data suggest that the size accuracy decreases as the density increases due to the difficulty in fabricating a high-density template. When the density goes above 1 Tb in^{-2}, the sigma increases significantly for every fabrication step.

Schmid *et al* [100] used a 0.25 Tb in^{-2} BPM template (50 nm feature period) to perform a JFIL imprint, and analysed the imprinted pattern. The mean dot period was 50 nm with a 1σ variation of 2.8%, the mean dot diameter was 36.3 nm with a 1σ variation of 6.1%. A similar experiment with an improved JFIL process performed by Ye *et al* [113] used a 1 Tb in^{-2} BPM template (27 nm feature period). They found a mean dot diameter of 16.6 nm with 1σ variation of 5.6%, and mean dot area of 216.2 nm^2 with 1σ variation of 9.8%. Xiao *et al* [99] performed DSA of PS-PDMS on prepatterned substrates, then transferred the patterns into quartz, although results for the spacing and size distributions following imprinting were not reported in this study. For 1 Tb in^{-2} the BCP 1σ spacing and size distributions were 3.9% and 5.0%, respectively, and after pattern transfer into quartz 4.6% and 5.1%, respectively. However, at 2 Tb in^{-2} the BCP spacing and size distributions were 5.5% and 6.7%, respectively, and after pattern transfer into quartz 8.2% and 7.4%, respectively, well outside the design tolerance of 5%. Albrecht *et al* [52] have fabricated hcp 1 Tb in^{-2} BPM using NIL, which after transfer into a magnetic film has demonstrated 1σ dot placement variation of 4.4%. One sample had a defect rate of 3×10^{-3}, and an intrinsic SFD of 10.4% (1σ). Although this was near the upper bound of the requirements, a bit error rate of 2×10^{-3} was still achieved when testing this sample with a read/write head. A separate sample had a defect rate of less than 10^{-3} and, due to improved magnetic film deposition and patterning techniques, an intrinsic SFD of just 4% (1σ), although this was not tested.

The results for 1 Tb in^{-2} indicate that this could become production ready in the near future. Higher areal densities will require significant further development to reduce variation and defectivity.

9.2. Throughput of NIL process

Industrial forecasts suggest that the market demand for hard disk recording media will reach 10^9 units per year in the next few years [114]. Patterned media throughput per machine is aimed at 1000 double-sided disks/hour [34]. 350 double-sided disks/hour production has been reported for the NuTera HD7000 machine [113]. A desirable target is that the total added cost for the entire patterned media process must not exceed \$1/disk [34]. However if a large areal density gain over alternatives can be achieved, this would allow more leeway than \$1/disk.

The main bottleneck to scaling up production rates is resist spread time, as leaving less time for the resist to spread leads to greater non-fill defectivity [120]. Reductions in spread time are being addressed through smaller resist drop volume, more accurate drop placement, and novel methods of fluid front control [34]. Elimination of hole tone templates by reverse tone processing also speeds up spread time, as imprinting with pillar tone templates leaves open channels for resist flow which are not present if imprinting with a hole tone template.

If the lifetime of a single imprint template is approximately 10^4 imprints, as might be anticipated [114], then a single master template can produce 10^4 daughter templates, which can then produce 10^8 disks. The replication of templates can be accomplished using the same NIL process used to produce the disks [114, 121]. An alternate method of template replication using Ni electroforming has also been investigated, due to its process durability and ease of making copies [122]. This has been demonstrated for a 0.8 Tb in^{-2} template, although a 2.5 Tb in^{-2} template could not be replicated because of the difficulty of nickel seed layer deposition in such small features [123].

Pattern inspection will need to occur at multiple points during the patterned media lithography process, beginning with the qualification of master templates. High resolution inspection equipment (e.g. electron microscopy) must be used to fully characterize the pattern quality on every master template. Long inspection times can be tolerated for master templates, which are critical to the lithography process. In contrast, replica templates and patterned disks will require short inspection times due to the much larger volume of substrates [114]. Large area techniques such as scatterometry can be used instead of high resolution inspections. These methods work well for patterned media, which contain simple and consistent patterns across the entire surface [34]. In addition completed patterned media disks will also be tested on magnetic spinstand testers for read/write capability, on an auditing basis (such as 1 out of every 100 disks) [4]. Figure 42 shows a potential BPM manufacturing flow with metrology carried out between various stages.

NIL has advanced a great deal in terms of defectivity and production rates, although further improvements are required before it is ready to enable mass production of BPM. That coupled with the massive capital investment in imprint machinery that would be required, means that it remains to be seen whether it will be adopted by the HDD industry for high volume manufacturing.
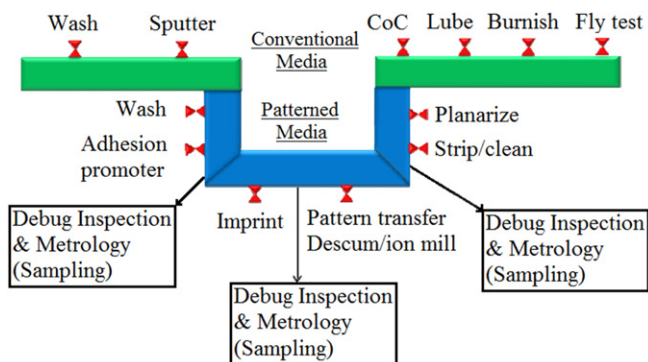
Figure 42. Potential BPM manufacturing flow. Reprinted with permission from [113]. Copyright 2011 Society of Photo Optical Instrumentation Engineers.

10. Conclusion

BPM shows potential to meet the continuing demand to increase the density of HDDs. One technique for the production of BPM is DSA BCP lithography. This process has the ability to create ordered arrays of magnetic bits on a macroscopic scale.

We have reviewed two techniques for directing the assembly of BCPs. The first technique of directing BCP assembly uses physical features, which is termed graphoepitaxy, and we have reviewed several methods for creating these features. Topographical posts provide 2D guidance and can enable very high density multiplication, reducing EBL write times, but it has not been demonstrated how both the posts and BCP components can be converted into topographically identical features on a NIL template. The use of shallow substrate features (e.g. ∼8 nm deep trenches) means that storage space is not compromised, but would result in the magnetic islands having height variations, which would present a problem for HDD operation. The use of deep trenches is currently the most promising method, as this can achieve circular tracks of magnetic islands without height variation. However, this method does compromise the resulting storage space. In addition, the absence of 2D guidance, and the LER of the trench walls present a significant obstacle to achieving 1σ dot position deviations of <5%.

The second technique reviewed was chemoepitaxy, where chemical regions patterned onto the surface direct the self-assembly of the BCPs. This technique provides 2D guidance, does not compromise storage space, and does not have the problem of LER seen with deep trenches. In addition, chemoepitaxy has been shown capable of creating rectangular bits with a BAR > 1 which are preferred to their cylindrical or spherical counterparts due to compatibility with existing head technology. However only modest density multiplication factors have been demonstrated, meaning a large amount of time, on the order of days, will still be required for EBL to pattern the surface. This will increase the cost and time taken to produce the resulting master template.

Graphoepitaxy is naturally more suited to the writing of servo patterns, due to the ability to write arbitrary trench patterns with EBL. For chemoepitaxy, only certain servo features such as a PES chevron pattern could be directly fabricated, whereas other servo marks would need to be servo-written onto regular bits, increasing manufacturing costs.

NIL is the leading candidate for mass production of BPM HDDs. Here improvements continue to be made in fabrication accuracy and throughput, although it is not yet certain whether these will be sufficient for mass production at densities beyond $1\,\mathrm{Tb\,in}^{-2}$.

Whilst graphoepitaxy has certain advantages, recent momentum in industry has been directed to developing a PS-PMMA chemoepitaxy process, forming submaster templates that can be combined to make high BAR islands. Recent results are encouraging, and suggest that high volume manufacturing of a BPM hard disk with storage between 1 and $2\,\mathrm{Tb\,in}^{-2}$ is close to becoming achievable. However, the competing technology of HAMR which uses conventional granular media could achieve similar densities. Some recent reports suggest that commercial HAMR devices may be available in 2016. However, working HAMR HDDs exceeding $1\,\mathrm{Tb\,in}^{-2}$ have not yet been convincingly demonstrated and significant difficulties remain. Hence BPM may ultimately prove competitive with HAMR for densities between 1 and $5\,\mathrm{Tb\,in}^{-2}$. In any case BPM offers the only currently viable route for densities above $5\,\mathrm{Tb\,in}^{-2}$ through the use of improved BCPs. Achieving working BPM at these densities will require significant further development of template fabrication, imprinting and transfer processes to achieve narrow position, size and switching field distributions but does offer the prospect of extending cost effective data storage based on HDDs into the future.

Acknowledgments

References

[1] Poulsen V 1899 *Danish Patent* No 2653
[2] Moser A 2002 Magnetic recording: advancing into the future *J. Phys. D: Appl. Phys.* **35** R157
[3] Fontana R E, Hetzler S R and Decad G 2012 Technology roadmap comparisons for TAPE, HDD, and NAND flash: implications for data storage applications *IEEE Trans. Magn.* **48** 1692–6
[4] Dobisz E A, Bandic Z Z, Wu T W and Albrecht T 2008 Patterned media: nanofabrication challenges of future disk drives *Proc. IEEE* **96** 1836–46
[5] Terris B D and Thomson T 2005 Nanofabricated and self-assembled magnetic structures as data storage media *J. Phys. D: Appl. Phys.* **38** R199–222
[6] Piramanayagam S N 2007 Perpendicular recording media for hard disk drives *J. Appl. Phys.* **102** 011301
[7] Piramanayagam S N and Srinivasan K 2009 Recording media research for future hard disk drives *J. Magn. Magn. Mater.* **321** 485–94
[8] Wood R 2000 The feasibility of magnetic recording at 1 Terabit per square inch *IEEE Trans. Magn.* **36** 36–42

J. Phys. D: Appl. Phys. **46** (2013) 503001

Topical Review

[9] Weller D and Moser A 1999 Thermal effect limits in ultrahigh-density magnetic recording *IEEE Trans. Magn.* **35** 4423–39

[10] Richter H J 2007 The transition from longitudinal to perpendicular recording *J. Phys. D: Appl. Phys.* **40** R149–77

[11] Kryder M H, Gage E C, McDaniel T W, Challener W A, Rottmayer R E, Ju G P, Hsia Y T and Erden M F 2008 Heat assisted magnetic recording *Proc. IEEE* **96** 1810–35

[12] Wang X B, Gao K Z, Zhou H, Itagi A, Seigler M and Gage E 2013 HAMR recording limitations and extendibility *IEEE Trans. Magn.* **49** 686–92

[13] Ross C 2001 Patterned magnetic recording media *Annu. Rev. Mater. Res.* **31** 203–35

[14] Shiroishi Y, Fukuda K, Tagawa I, Iwasaki H, Takenoiri S, Tanaka H, Mutoh H and Yoshikawa N 2009 Future options for HDD storage *IEEE Trans. Magn.* **45** 3816–22

[15] Richter H J, Lyberatos A, Nowak U, Evans R F L and Chantrell R W 2012 The thermodynamic limits of magnetic recording *J. Appl. Phys.* **111** 033909

[16] McDaniel T W 2012 Areal density limitation in bit-patterned, heat-assisted magnetic recording using FePtX media *J. Appl. Phys.* **112** 093920

[17] McDaniel T W 2005 Ultimate limits to thermally assisted magnetic recording *J. Phys.: Condens. Matter* **17** R315–32

[18] Lille J, Patel K, Ruiz R, Wu T W, Gao H, Wan L, Zeltzer G, Dobisz E and Albrecht T R 2011 Imprint lithography template technology for bit patterned media (BPM) *Photomask Technology 2011* vol 8166 ed W Maurer and F E Abboud (Bellingham, WA: SPIE-International Society of Optical Engineering) *Proc. SPIE* 816626

[19] Richter H J *et al* 2006 Recording potential of bit-patterned media *Appl. Phys. Lett.* **88** 222512

[20] Schabes M E 2008 Micromagnetic simulations for terabit/in^2 head/media systems *J. Magn. Magn. Mater.* **320** 2880–4

[21] Thomson T, Hu G and Terris B D 2006 Intrinsic distribution of magnetic anisotropy in thin films probed by patterned nanostructures *Phys. Rev. Lett.* **96** 257204

[22] Shaw J M, Rippard W H, Russek S E, Reith T and Falco C M 2007 Origins of switching field distributions in perpendicular magnetic nanodot arrays *J. Appl. Phys.* **101** 023909

[23] Hellwig O, Berger A, Thomson T, Dobisz E, Bandic Z Z, Yang H, Kercher D S and Fullerton E E 2007 Separating dipolar broadening from the intrinsic switching field distribution in perpendicular patterned media *Appl. Phys. Lett.* **90** 162516

[24] Kanda K *et al* 2013 A 19 nm 112.8 mm(2) 64 Gb multi-level flash memory with 400 Mbit/sec/pin 1.8 V toggle mode interface *IEEE J. Solid-State Circuits* **48** 1590–67

[25] Wagner C and Harned N 2010 EUV lithography: lithography gets extreme *Nature Photon.* **4** 24–6

[26] Albrecht T R *et al* 2013 Generation and transfer of large area lithographic patterns in the ~10 nm feature size regime *SPIE Advanced Lithography Conf. (San Jose, CA)*

[27] Solak H H and Ekinci Y 2007 Bit-array patterns with density over 1 Tbit/in.^{2} fabricated by extreme ultraviolet interference lithography *J. Vac. Sci. Technol.* B **25** 2123–6

[28] Auzelyte V *et al* 2009 Extreme ultraviolet interference lithography at the Paul Scherrer Institut *J. Micro-Nanolithogr. MEMS and MOEMS* **8** 021204

[29] Sarkar S S, Solak H H, Raabe J, David C and van der Veen J F 2010 Fabrication of Fresnel zone plates with 25 nm zone width using extreme ultraviolet holography *Microelectron. Eng.* **87** 854–8

[30] Yang X, Xiao S, Wu W, Xu Y, Mountfield K, Rottmayer R, Lee K, Kuo D and Weller D 2007 Challenges in 1 Teradot/inch^2 dot patterning using electron beam lithography for bit-patterned media *J. Vac. Sci. Technol.* B **25** 2202–9

[31] Vieu C, Carcenac F, Pepin A, Chen Y, Mejias M, Lebib A, Manin-Ferlazzo L, Couraud L and Launois H 2000 Electron beam lithography: resolution limits and applications *Appl. Surf. Sci.* **164** 111–7

[32] Manfrinato V R, Zhang L, Su D, Duan H, Hobbs R G, Stach E A and Berggren K K 2013 Resolution limits of electron-beam lithography toward the atomic scale *Nano Lett.* **13** 1555–58

[33] Chang T H P 1975 Proximity effect in electron-beam lithography *J. Vac. Sci. Technol.* **12** 1271–5

[34] Malloy M and Litt L C 2011 Technology review and assessment of nanoimprint lithography for semiconductor and patterned media manufacturing *J. Micro-Nanolithogr. MEMS and MOEMS* **10** 032001

[35] Chou S Y, Krauss P R and Renstrom P J 1996 Nanoimprint lithography *J. Vac. Sci. Technol.* B **14** 4129–33

[36] Bailey T, Choi B J, Colburn M, Meissl M, Shaya S, Ekerdt J G, Sreenivasan S V and Willson C G 2000 Step and flash imprint lithography: template surface treatment and defect analysis *J. Vac. Sci. Technol.* B **18** 3572–7

[37] Schift H 2008 Nanoimprint lithography: an old story in modern times? a review *J. Vac. Sci. Technol.* B **26** 458–80

[38] Whitesides G M and Grzybowski B 2002 Self-assembly at all scales *Science* **295** 2418–21

[39] Yang X, Wan L, Xiao S, Xu Y and Weller D K 2009 Directed block copolymer assembly versus electron beam lithography for bit-patterned media with areal density of 1 Terabit/inch^2 and beyond *ACS Nano* **3** 1844–58

[40] Xiao S, Yang X, Park S, Weller D and Russell T P 2009 A novel approach to addressable 4 Teradot/in^2 patterned media *Adv. Mater.* **21** 2516–9

[41] Lodge T P 2003 Block copolymers: past successes and future challenges *Macromol. Chem. Phys.* **204** 265–273

[42] Zhao D, Huo Q, Feng J, Chmelka B F and Stucky G D 1998 Nonionic triblock and star diblock copolymer and oligomeric surfactant syntheses of highly ordered, hydrothermally stable, mesoporous silica structures *J. Am. Chem. Soc.* **120** 6024–36

[43] Pochan D J, Chen Z, Cui H, Hales K, Qi K and Wooley K L 2004 Toroidal triblock copolymer assemblies *Science* **306** 94–7

[44] Nardin C, Hirt T, Leukel J and Meier W 1999 Polymerized ABA triblock copolymer vesicles *Langmuir* **16** 1035–41

[45] Ni Y, Rulkens R and Manners I 1996 Transition metal-based polymers with controlled architectures: well-defined poly(ferrocenylsilane) homopolymers and multiblock copolymers via the living anionic ring-opening polymerization of silicon-bridged [1]ferrocenophanes *J. Am. Chem. Soc.* **118** 4102–14

[46] Ross C and Cheng J 2008 Patterned magnetic media made by self-assembled block-copolymer lithography *MRS Bull.* **33** 838–45

[47] Ross C A 2007 Self-assembled resists for nanolithography *Microlithogr. World* **16** 4

[48] Bates F S and Fredrickson G H 1990 Block copolymer thermodynamics: theory and experiment *Annu. Rev. Phys. Chem.* **41** 525–57

[49] Patel K C, Ruiz R, Lille J, Wan L, Dobisz E, Gao H, Robertson N, and Albrecht T R 2012 Line frequency doubling of directed self assembly patterns for single-digit bit pattern media lithography *Alternative Lithographic Technologies IV* vol 8323 ed W M Tong and D J Resnick (Bellingham, WA: SPIE-International Society of Optical Engineering) 8323OU

[50] Russell T P, Hjelm R P and Seeger P A 1990 Temperature dependence of the interaction parameter of polystyrene and poly(methyl methacrylate) *Macromolecules* **23** 890–3

[51] Chevalier X *et al* 2013 Scaling-down lithographic dimensions with block-copolymer materials: 10 nm-sized features with PS-b-PMMA *Alternative Lithographic Technologies V* vol 8680 ed W M Tong and D J Resnick (Bellingham, WA: SPIE-International Society of Optical Engineering) 031102

[52] Albrecht T R *et al* 2013 Bit patterned media at 1 Tdot/in^2 and beyond *IEEE Trans. Magn.* **49** 773–8

[53] Cheng J Y, Ross C A, Smith H I and Thomas E L 2006 Templated self-assembly of block copolymers: top-down helps bottom-up *Adv. Mater.* **18** 2505–21

[54] Tseng Y C and Darling S B 2010 Block copolymer nanostructures for technology *Polymers* **2** 470–89

[55] Biswas A, Bayer I S, Biris A S, Wang T, Dervishi E and Faupel F 2012 Advances in top-down and bottom-up surface nanofabrication: techniques, applications & future prospects *Adv. Colloid Interface Sci.* **170** 2–27

[56] Albrecht T R, Hellwing O, Ruiz R, Schabes M E, Terris B D and Wu X Z 2009 *Bit-Patterned Magnetic Recording: Nanoscale Magnetic Islands for Data Storage Nanoscale Mag. Mater. Appl.* 237–74

[57] Berry B C, Bosse A W, Douglas J F, Jones R L and Karim A 2007 Orientational order in block copolymer films zone annealed below the order-disorder transition temperature *Nano Lett.* **7** 2789–94

[58] Morkved T L, Lu M, Urbas A M, Ehrichs E E, Jaeger H M, Mansky P and Russell T P 1996 Local control of microdomain orientation in diblock copolymer thin films with electric fields *Science* **273** 931–3

[59] Hadziioannou G, Mathis A and Skoulios A 1979 Synthesis of 3-block styrene-isoprene-styrene copolymer single-crystals via plane shear-flow *Colloid Polym. Sci.* **257** 136–9

[60] De Rosa C, Park C, Thomas E L and Lotz B 2000 Microdomain patterns from directional eutectic solidification and epitaxy *Nature* **405** 433–7

[61] Darling S B 2007 Directing the self-assembly of block copolymers *Prog. Polym. Sci.* **32** 1152–204

[62] Ruiz R, Kang H, Detcheverry F A, Dobisz E, Kercher D S, Albrecht T R, de Pablo J J and Nealey P F 2008 Density multiplication and improved lithography by directed block copolymer assembly *Science* **321** 936–9

[63] Thurn-Albrecht T, Steiner R, DeRouchey J, Stafford C M, Huang E, Bal M, Tuominen M, Hawker C J and Russell T 2000 Nanoscopic templates from oriented block copolymer films *Adv. Mater.* **12** 787–91

[64] Naito K, Hieda H, Sakurai M, Kamata Y and Asakawa K 2002 2.5-inch disk patterned media prepared by an artificially assisted self-assembling method *Magn. IEEE Trans.* **38** 1949–51

[65] Ting Y H, Park S M, Liu C C, Liu X S, Himpsel F J, Nealey P F and Wendt A E 2008 Plasma etch removal of poly(methyl methacrylate) in block copolymer lithography *J. Vac. Sci. Technol.* B **26** 1684–9

[66] Xiao S G, Yang X M, Edwards E W, La Y H and Nealey P F 2005 Graphoepitaxy of cylinder-forming block copolymers for use as templates to pattern magnetic metal dot arrays *Nanotechnology* **16** S324–9

[67] Cheng J Y, Ross C A, Chan V Z H, Thomas E L, Lammertink R G H and Vancso G J 2001 Formation of a cobalt magnetic dot array via block copolymer lithography *Adv. Mater.* **13** 1174–8

[68] Hu G, Thomson T, Albrecht M, Best M E, Terris B D, Rettner C T, Raoux S, McClelland G M and Hart M W 2004 Magnetic and recording properties of Co/Pd islands on prepatterned substrates *J. Appl. Phys.* **95** 7013–5

[69] Wan L, Ruiz R, Gao H, Patel K C, Lille J, Zeltzer G, Dobisz E A, Bogdanov A, Nealey P F and Albrecht T R 2012 Fabrication of templates with rectangular bits on circular tracks by combining block copolymer directed self-assembly and nanoimprint lithography *J. Micro-Nanolithogr. MEMS and MOEMS* **11** 031405

[70] Tseng Y C, Peng Q, Ocola L E, Elam J W, and Darling S B 2011 Enhanced block copolymer lithography using sequential infiltration synthesis *J. Phys. Chem.* C **115** 17725–9

[71] Tseng Y C, Mane A U, Elam J W and Darling S B 2012 Enhanced lithographic imaging layer meets semiconductor manufacturing specification a decade early *Adv. Mater.* **24** 2608–13

[72] Peng Q, Tseng Y C, Darling S B and Elam J W 2010 Nanoscopic patterned Materials with tunable dimensions via atomic layer deposition on block copolymers *Adv. Mater.* **22** 5129–33

[73] Peng Q, Tseng Y C, Darling S B and Elam J W 2011 A route to nanoscopic materials via sequential infiltration synthesis on block copolymer templates *Acs Nano* **5** 4600–6

[74] Tseng Y C, Peng Q, Ocola L E, Czaplewski D A, Elam J W and Darling S B 2011 Enhanced polymeric lithography resists via sequential infiltration synthesis *J. Mater. Chem.* **21** 11722–5

[75] Ruiz R, Wan L, Lille J, Patel K C, Dobisz E, Johnston D E, Kisslinger K and Black C T 2012 Image quality and pattern transfer in directed self assembly with block-selective atomic layer deposition *J. Vac. Sci. Technol.* B **30** 06F202

[76] Moser A, Hellwig O, Kercher D and Dobisz E 2007 Off-track margin in bit patterned media *Appl. Phys. Lett.* **91** 162502

[77] Dusa M *et al* 2007 Pitch doubling through dual patterning lithography challenges in integration and litho budgets—art. no. 65200G *Optical Microlithography XX, Pts 1-3* vol 6520 ed D G Flagello (Bellingham, WA: SPIE-International Society of Optical Engineering) p G5200

[78] Jung W Y, Kim S M, Kim C D, Sim G H, Jeon S M, Park S W, B S Lee, Park S K, Kim J S and Heon L S 2007 Patterning with amorphous carbon spacer for expanding the resolution limit of current lithography tool—art. no. 65201C *Optical Microlithography XX, Pts 1-3* vol 6520 ed D G Flagello (Bellingham, WA: SPIE-International Society of Optical Engineering) p C5201

[79] Cheng J Y, Mayes A M and Ross C A 2004 Nanostructure engineering by templated self-assembly of block copolymers *Nature Mater.* **3** 823–8

[80] Kamata Y, Kikitsu A, Hieda H, Sakurai M, Naito K, Bai J M and Ishio S 2007 Microscopic magnetic characteristics of CoCrPt-patterned media made by artificially aligned self-organized mask *Japan. J. Appl. Phys. Part 1-Regular Papers Brief Communications & Review Papers* **46** 999–1002

[81] Kikitsu A, Maeda T, Hieda H, Yamamoto R, Kihara N and Kamata Y 2013 5 Tdots/in^2 bit patterned media fabricated by a directed self-assembly mask *IEEE Trans. Magn.* **49** 693–8

[82] Segalman R A, Yokoyama H and Kramer E J 2001 Graphoepitaxy of spherical domain block copolymer films *Adv. Mater.* **13** 1152–5

[83] Bita I, Yang J K W, Jung Y S, Ross C A, Thomas E L and Berggren K K 2008 Graphoepitaxy of self-assembled block copolymers on two-dimensional periodic patterned templates *Science* **321** 939–43

[84] Chang J B, Son J G, Hannon A F, Alexander-Katz A, Ross C A and Berggren K K 2012 Aligned sub-10-nm block copolymer patterns templated by post arrays *Acs Nano* **6** 2071–7

[85] Edwards E W, Montague M F, Solak H H, Hawker C J and Nealey P F 2004 Precise control over molecular

J. Phys. D: Appl. Phys. **46** (2013) 503001

Topical Review

dimensions of block-copolymer domains using the interfacial energy of chemically nanopatterned substrates *Adv. Mater.* **16** 1315–9

[86] Li W H, Xie N, Qiu F, Yang Y L and Shi A C 2011 Ordering kinetics of block copolymers directed by periodic two-dimensional rectangular fields *J. Chem. Phys.* **134** 144901

[87] Tang Q Y and Ma Y Q 2010 High density multiplication of graphoepitaxy directed block copolymer assembly on two-dimensional lattice template *Soft Matter* **6** 4460–5

[88] Hong S W, Gu X, Huh J, Xiao S and Russell T P 2011 Circular nanopatterns over large areas from the self-assembly of block copolymers guided by shallow trenches *Acs Nano* **5** 2855–60

[89] Park S, Lee D H, Xu J, Kim B, Hong S W, Jeong U, Xu T and Russell T P 2009 Macroscopic 10-terabit-per-square-inch arrays from block copolymers with lateral order *Science* **323** 1030–3

[90] Jung Y S, Jung W and Ross C A 2008 Nanofabricated concentric ring structures by templated self-assembly of a diblock copolymer *Nano Lett.* **8** 2975–81

[91] Wang H, Zhao H B, Rahman T, Isowaki Y, Kamata Y, Maeda T, Hieda H, Kikitsu A and Wang J P 2013 Fabrication and characterization of FePt exchange coupled composite and graded bit patterned media *IEEE Trans. Magn.* **49** 707–12

[92] Kim S O, Solak H H, Stoykovich M P, Ferrier N J, de Pablo J J and Nealey P F 2003 Epitaxial self-assembly of block copolymers on lithographically defined nanopatterned substrates *Nature* **424** 411–4

[93] Tada Y, Akasaka S, Takenaka M, Yoshida H, Ruiz R, Dobisz E and Hasegawa H 2009 Nine-fold density multiplication of hcp lattice pattern by directed self-assembly of block copolymer *Polymer* **50** 4250–6

[94] Tada Y, Akasaka S, Yoshida H, Hasegawa H, Dobisz E, Kercher D and Takenaka M 2008 Directed self-assembly of diblock copolymer thin films on chemically-patterned substrates for defect-free nano-patterning *Macromolecules* **41** 9267–76

[95] Wan L and Yang X 2009 Directed self-assembly of cylinder-forming block copolymers: prepatterning effect on pattern quality and density multiplication factor *Langmuir* **25** 12408–13

[96] Cheng J Y, Rettner C T, Sanders D P, Kim H-C and Hinsberg W D 2008 Dense self-assembly on sparse chemical patterns: rectifying and multiplying lithographic patterns using block copolymers *Adv. Mater.* **20** 3155–8

[97] Ruiz R, Dobisz E and Albrecht T R 2011 Rectangular patterns using block copolymer directed assembly for high bit aspect ratio patterned media *Acs Nano* **5** 79–84

[98] Xiao S A G, Yang X M, Lee K Y, ver der Veerdonk R J M, Kuo D and Russell T P 2011 Aligned nanowires and nanodots by directed block copolymer assembly *Nanotechnology* **22** 305302

[99] Xiao S, Yang X, Lee K Y, Hwu J J, Wago K and Kuo D 2013 Directed self-assembly for high-density bit-patterned media fabrication using spherical block copolymers *J. Micro/Nanolithogr. MEMS and MOEMS* **12** 031110

[100] Schmid G M *et al* 2009 Step and flash imprint lithography for manufacturing patterned media *J. Vac. Sci. Technol.* B **27** 573–80

[101] Lille J *et al* 2012 Integration of servo and high bit aspect ratio data patterns on nanoimprint templates for patterned media *IEEE Trans. Magn.* **48** 2757–60

[102] Hadjichristidis N, Pispas S and Floudas G 2002 *Block Copolymers: Synthetic Strategies, Physical Properties, and Applications* (New York: Wiley)

[103] Liu G L, Nealey P F, Ruiz R, Dobisz E, Patel K C and Albrecht T R 2011 Fabrication of chevron patterns for patterned media with block copolymer directed assembly *J. Vac. Sci. Technol.* B **29** 06F204

[104] Kihara N, Yamamoto R, Sasao N, Shimada T, Yuzawa A, Okino T, Ootera Y, Kamata Y and Kikitsu A 2012 Fabrication of 5 Tdot/in.^{2} bit patterned media with servo pattern using directed self-assembly *J. Vac. Sci. Technol.* B **30** 06FH02

[105] Hughes E C and Messner W C 2003 New servo pattern for hard disk storage using pattern media *J. Appl. Phys.* **93** 7002–4

[106] Lin X D, Zhu J G and Messner W 2000 Investigation of advanced position error signal patterns in patterned media *J. Appl. Phys.* **87** 5117–9

[107] Kamata Y, Kikitsu A, Kihara N, Morita S, Kimura K and Izumi H 2011 Fabrication of ridge-and-groove servo pattern consisting of self-assembled dots for 2.5 Tb/in^2 bit patterned media *IEEE Trans. Magn.* **47** 51–4

[108] Han Y and de Callafon R A 2009 Evaluating track-following servo performance of high-density hard disk drives using patterned media *IEEE Trans. Magn.* **45** 5352–9

[109] Yamamoto R, Yuzawa A, Shimada T, Ootera Y, Kamata Y, Kihara N and Kikitsu A 2012 Nanoimprint mold for 2.5 Tbit/in.^{2} directed self-assembly bit patterned media with phase servo pattern *Japan. J. Appl. Phys.* **51** 046503

[110] Yang X M, Xu Y, Seiler C, Wan L and Xiao S G 2008 Toward 1 Tdot/in.^{2} nanoimprint lithography for magnetic bit-patterned media: opportunities and challenges *J. Vac. Sci. Technol.* B **26** 2604–10

[111] Singhal S, Attota R and Sreenivasan S V 2012 Residual layer thickness control and metrology in jet and flash imprint lithography *Metrology, Inspection, and Process Control for Microlithography XXVI, Pts 1 and 2* vol 8324 ed A Starikov (Bellingham, WA: SPIE-International Society of Optical Engineering) 832434

[112] Singh L, Luo K, Ye Z M, Xu F, Haase G, Curran D, LaBrake D, Resnick D and Sreenivasan S V 2011 Defect reduction of high-density full-field patterns in jet and flash imprint lithography *J. Micro/Nanolithogr. MEMS and MOEMS* **10** 033018

[113] Ye Z M, Ramos R, Brooks C, Simpson L, Fretwell J, Carden S, Hellebrekers P, LaBrake D, Resnick D J and Sreenivasan S V 2011 High density patterned media fabrication using jet and flash imprint lithography *Alternative Lithographic Technologies III* vol 7970 ed D J C Herr (Bellingham, WA: SPIE-International Society of Optical Engineering) 79700L

[114] Schmid G, Brooks C, Ye Z, Johnson S, LaBrake D, Sreenivasan S V and Resnick D 2009 Jet and flash imprint lithography for the fabrication of patterned media drives *SPIE Proc.* **7488** 748820

[115] Ye Z M, Carden S, Hellebrekers P, LaBrake D, Resnick D J, Melliar-Smith M and Sreenivasan S V 2012 Imprint process performance for patterned media at densities greater than 1 Tb/in^2 *Alternative Lithographic Technologies IV* vol 8323 ed W M Tong and D J Resnick (Bellingham, WA: SPIE-International Society of Optical Engineering) 8323OV

[116] Dauksher W J, Le N V, Gehoski K A, Ainley E S, Nordquist K J and Joshi N 2007 An electrical defectivity characterization of wafers imprinted with step and flash imprint lithography—art. no. 651714 *Emerging Lithographic Technologies XI, Pts 1 and 2* vol 6517 ed M J Lercel (Bellingham, WA: SPIE-International Society of Optical Engineering) 651714

28

[117] Long B K, Keitz B K and Willson C G 2007 Materials for
        step and flash imprint lithography (S-FIL (R)) *J. Mater.
        Chem.* **17** 3575–80
[118] Singh S, Chen S W, Dress P, Kurataka N, Gauzner G and
        Dietze U 2010 Advanced cleaning of nano-imprint
        lithography template in patterned media applications
        Photomask Technology 2010 vol 7823
        ed M W Montgomery and W Maurer (Bellingham, WA:
        SPIE-International Society of Optical Engineering)
        78232T
[119] Yang X M, Xu Y, Lee K, Xiao S G, Ku D and
        Weller D 2009 Advanced lithography for
        bit patterned media *IEEE Trans. Magn.*
        45 833–8
[120] Malloy M and Litt L C 2010 Step and flash imprint
        lithography for semiconductor high volume
        manufacturing? *Alternative Lithographic Technologies II*
        vol 7637 ed D J C Herr (Bellingham, WA:
        SPIE-International Society of Optical Engineering)
        763706

[121] Selinidis K S, Brooks C B, Doyle G F, Brown L, Jones C,
        Imhof J, LaBrake D L, Resnick D J and Sreenivasan S V
        2011 Progress in mask replication using jet and flash
        imprint lithography *Alternative Lithographic Technologies
        III* vol 7970 ed D J C Herr (Bellingham, WA:
        SPIE-International Society of Optical Engineering)
        797009
[122] Kihara N, Hieda H and Naito K 2008 NIL mold
        manufacturing using self-organized diblock copolymer as
        patterning template—art. no. 692126 *Emerging
        Lithographic Technologies XII, Pts 1 and 2* vol 6921
        ed F M Schellenberg (Bellingham, WA: SPIE-International
        Society of Optical Engineering) 692126
[123] Ootera Y, Yuzawa A, Shimada T, Yamamoto R, Kamata Y,
        Kihara N and Kikitsu A 2011 Nanoimprint process for
        2.5 Tb/in^2 bit patterned media fabricated by
        self-assembling method, in *Alternative Lithographic
        Technologies III* vol 7970 ed D J C Herr (Bellingham, WA:
        SPIE-International Society of Optical Engineering)
        7970OK